

Small- x Asymptotics of the Gluon Helicity Distribution

Yuri V. Kovchegov*

Department of Physics, The Ohio State University, Columbus, OH 43210, USA

Daniel Pitonyak†

Division of Science, Penn State University-Berks, Reading, PA 19610, USA

Matthew D. Sievert‡

Theoretical Division, Los Alamos National Laboratory, Los Alamos, NM 87545, USA

We determine the small- x asymptotics of the gluon helicity distribution in a proton at leading order in perturbative QCD at large N_c . To achieve this, we begin by evaluating the dipole gluon helicity TMD at small x . In the process we obtain an interesting new result: in contrast to the unpolarized dipole gluon TMD case, the operator governing the small- x behavior of the dipole gluon helicity TMD is different from the operator corresponding to the polarized dipole scattering amplitude (used in our previous work to determine the small- x asymptotics of the quark helicity distribution). We then construct and solve novel small- x large- N_c evolution equations for the operator related to the dipole gluon helicity TMD. Our main result is the small- x asymptotics for the gluon helicity distribution: $\Delta G \sim (\frac{1}{x})^{\alpha_h^G}$ with $\alpha_h^G = \frac{13}{4\sqrt{3}} \sqrt{\frac{\alpha_s N_c}{2\pi}} \approx 1.88 \sqrt{\frac{\alpha_s N_c}{2\pi}}$. We note that the power α_h^G is approximately 20% lower than the corresponding power α_h^q for the small- x asymptotics of the quark helicity distribution defined by $\Delta q \sim (\frac{1}{x})^{\alpha_h^q}$ with $\alpha_h^q = \frac{4}{\sqrt{3}} \sqrt{\frac{\alpha_s N_c}{2\pi}} \approx 2.31 \sqrt{\frac{\alpha_s N_c}{2\pi}}$ found in our earlier work.

PACS numbers: 12.38.-t, 12.38.Bx, 12.38.Cy

I. INTRODUCTION

A solid theoretical understanding of the small- x asymptotics of the quark and gluon helicity distributions $\Delta q(x, Q^2)$ and $\Delta G(x, Q^2)$ is crucially important for the resolution of the proton spin puzzle. The quark and gluon components of the proton spin,

$$S_q(Q^2) = \frac{1}{2} \int_0^1 dx \Delta \Sigma(x, Q^2) \quad \text{and} \quad S_G(Q^2) = \int_0^1 dx \Delta G(x, Q^2), \quad (1)$$

may receive significant contributions from the small- x region. Given that the current experimental values (see [1–4] for reviews), $S_q(Q^2 = 10 \text{ GeV}^2) \approx 0.15 \div 0.20$ (integrated over $0.001 < x < 1$) and $S_G(Q^2 = 10 \text{ GeV}^2) \approx 0.13 \div 0.26$ (integrated over $0.05 < x < 1$), still do not add up to the proton spin of $1/2$, the small- x region may turn out to be important for satisfying helicity sum rules [5–7] (see [8] for a review), such as the Jaffe–Manohar sum rule [5]

$$S_q + L_q + S_G + L_G = \frac{1}{2}, \quad (2)$$

where L_q and L_G denote the quark and gluon orbital angular momentum (OAM), respectively.

Moreover, the experimental measurement of the relevant double-longitudinal spin asymmetry A_{LL} is always limited to the $x \in [x_{min}, 1]$ subset of the $x \in [0, 1]$ range employed in the integrals of Eq. (1), with x_{min} given by the experimental coverage of the specific machine and detector. No matter how high-energy an experiment may be, there will always be some x_{min} below which it will not be able to measure A_{LL} . Therefore, below that x_{min} one does not have data from which to extract $\Delta q(x, Q^2)$ and $\Delta G(x, Q^2)$. To be certain that the experimentally excluded region of $x \in [0, x_{min}]$ does not contribute much to S_q and S_G , or to obtain an accurate estimate of how much spin resides at $x \in [0, x_{min}]$, one has to develop a quantitative theoretical understanding of $\Delta q(x, Q^2)$ and $\Delta G(x, Q^2)$ at small x . Then one could hope for the following possible scenario at future polarized-scattering experiments, such as the ones to be carried out at the proposed Electron-Ion Collider (EIC) in the US [1]: one may obtain solid agreement

* Email: kovchegov.1@osu.edu

† Email: dap67@psu.edu

‡ Email: sievertmd@lanl.gov

between theory predictions and experiment for the x -dependence of A_{LL} above x_{min} (but still at small x), that is for $x \gtrsim x_{min}$, which would allow one to confidently extrapolate $\Delta q(x, Q^2)$ and $\Delta G(x, Q^2)$ to the $x < x_{min}$ region. This extrapolation, in turn, would allow one to make a good estimate of the amount of the proton's spin carried by the quarks and gluons at $x < x_{min}$. The extrapolation would need to be further tested by later experiments probing polarization at smaller values of x : if agreement is found again, one may be able claim that the procedure is converging and that the spin at small x is approaching full theoretical control.

To address the important question of the small- x asymptotics of $\Delta q(x, Q^2)$ in the flavor-singlet channel, we derived small- x helicity evolution equations in [9]. The evolution equations were written down for the polarized dipole amplitude, which can be defined as the part of the forward scattering amplitude for a $q\bar{q}$ dipole, with a longitudinally polarized quark or antiquark in it, on a longitudinally polarized target proton that depends on the product of the target and projectile polarizations. The polarized dipole amplitude is related to the quark helicity transverse-momentum-dependent (TMD) parton distribution function: knowing the former gives us the latter [10]. The evolution equations for the polarized dipole amplitude are both similar to and different from the unpolarized Balitsky–Kovchegov (BK) [11–14] and Jalilian-Marian–Iancu–McLerran–Weigert–Leonidov–Kovner (JIMWLK) [15–18] evolution equations. The similarity is in the fact that both the helicity evolution and BK/JIMWLK evolution involve Wilson lines. Moreover, just like in the Balitsky hierarchy [11, 12], the helicity evolution equations do not close in general, and the large- N_c limit has to be invoked to produce a closed equation [11–14]. There are also important differences: helicity evolution is sub-eikonal, and involves the so-called “polarized Wilson line” operator, which is related to the helicity-dependent part of a high-energy polarized-quark propagator through a longitudinally polarized target [9]. The helicity evolution equations also become a closed system of equations in the large- N_c & N_f limit, in addition to the large- N_c limit.

Perhaps most importantly, the helicity evolution equations resum *double logarithms* of energy, that is, powers of $\alpha_s \ln^2 \frac{1}{x}$ with α_s the strong coupling constant. This is in contrast to the leading-logarithmic resummation of the powers of $\alpha_s \ln \frac{1}{x}$ in the unpolarized Balitsky–Fadin–Kuraev–Lipatov (BFKL) [19, 20] along with the BK/JIMWLK equations. The double-logarithmic approximation (DLA) resulting from resumming the powers of $\alpha_s \ln^2 \frac{1}{x}$ was considered before for the t -channel quark exchange amplitudes [21–27]. For helicity evolution it was first applied by Bartels, Ermolaev and Ryskin (BER) in [28, 29] (see also [30–33]). (The DLA parameter $\alpha_s \ln^2 \frac{1}{x}$ does not exist in the unpolarized BFKL/BK/JIMWLK evolution, and so far has been established either in t -channel quark exchanges [21–27] or for the t -channel longitudinal spin transfer [28, 29].) To accomplish the DLA resummation in the s -channel small- x formalism we had to introduce an auxiliary “neighbor” polarized dipole amplitude [9], which was never required in the leading-logarithmic unpolarized dipole evolution [11–14, 34–36].

The derivation of the flavor-singlet helicity evolution equations from [9] was further clarified in [37], where we also derived and solved the evolution equation for the quark helicity TMD in the flavor non-singlet case. The resulting small- x (large- N_c) asymptotics of the flavor non-singlet quark helicity distribution were in complete agreement with that derived previously by BER [28].

The flavor-singlet large- N_c helicity evolution equations from [9] were first solved numerically in [38] and then analytically in [39]. The resulting small- x asymptotics of the quark helicity parton distribution function (PDF) were found to be

$$\Delta q(x, Q^2) \sim \left(\frac{1}{x}\right)^{\alpha_h^q} \quad \text{with} \quad \alpha_h^q = \frac{4}{\sqrt{3}} \sqrt{\frac{\alpha_s N_c}{2\pi}} \approx 2.31 \sqrt{\frac{\alpha_s N_c}{2\pi}}. \quad (3)$$

The flavor-singlet quark helicity intercept α_h^q at large N_c was about 30% smaller than that found by BER in [29]. We discussed the possible origin of our differences in [37]; in Appendix B of that paper we presented some of the DLA diagram contributions we believe BER did not include in their analysis.

Having established the small- x asymptotics for the quark helicity distribution (3), we now turn our attention to the gluon helicity distribution, which is the main topic of this paper. We begin in Sec. II by reviewing the central results from the quark helicity case and by constructing a definition for the “polarized Wilson line” operator employed previously in [9, 37] without presenting an explicit form. The polarized Wilson line operator provides us with the operatorial form of the polarized dipole scattering amplitude from [9, 37]. We proceed in Sec. III by evaluating the gluon helicity TMDs at small x . We consider both the dipole and Weizsäcker-Williams (WW) gluon helicity TMDs according to the standard prescription [40]. Starting with their definitions, we express each of those gluon helicity TMDs in terms of light-cone Wilson lines and an insertion of the sub-eikonal longitudinal spin-dependent gluon field of the target. In [40] a similar procedure expressed the unpolarized dipole gluon TMD in terms of the forward scattering amplitude for a (fundamental) $q\bar{q}$ dipole scattering on the target, hence giving rise to the name for the dipole TMD. (Also see Ref. [41] for related work on the distribution of linearly polarized gluons.) This amplitude can be found by solving the BK evolution equation. Surprisingly, and unlike the unpolarized case, the dipole gluon helicity TMD turns out not to be directly related to the polarized dipole scattering amplitude. Instead it is related to a somewhat different operator as shown in Sec. III. (The same applies for the WW gluon helicity TMD: it is not directly related to the polarized dipole amplitude. However, this is not unlike the unpolarized case, in which the unpolarized WW gluon TMD was found to be related to the color-quadrupole amplitude [42] and not to the dipole one.)

The small- x evolution for the dipole gluon helicity TMD is constructed in Sec. IV. There we begin by reconstructing the DLA evolution equations for the polarized dipole amplitude from [9]; since now we have an operator expression for the polarized dipole amplitude, we use the operator language, similar to that developed by Balitsky in [11, 12]. This is a cross-check of both our equations in [9] as well as the operator definition and approach. We proceed by applying the operator method to evaluate the operator related to the dipole gluon helicity TMD. The result, in the large- N_c limit, is the evolution equations (96) which mix this “gluon helicity operator” with the “quark helicity operator” given by the polarized dipole amplitude. These equations are solved in Sec. V, both analytically and numerically. The end result is the following small- x asymptotics of the gluon helicity distribution:

$$\Delta G(x, Q^2) \sim \left(\frac{1}{x}\right)^{\alpha_h^G} \quad \text{with} \quad \alpha_h^G = \frac{13}{4\sqrt{3}} \sqrt{\frac{\alpha_s N_c}{2\pi}} \approx 1.88 \sqrt{\frac{\alpha_s N_c}{2\pi}}. \quad (4)$$

Equations (3) and (4) give us the leading-in- α_s small- x asymptotics of both the quark and gluon helicity distributions. It is interesting to note that $\alpha_h^G < \alpha_h^q$; we explore the phenomenological consequences of this in Sec. VI and Sec. VII.

In Sec. VI we estimate the amount of the proton’s spin carried by small- x gluons using a simple phenomenological approach. As depicted in Fig. 9, we observe a $5 \div 10\%$ increase in the amount of gluon spin if we use our intercept (4) to augment the existing DSSV14 [43] PDF parameterization. We also discuss the importance of incorporating our work into future fits of helicity PDFs.

We conclude in Sec. VII by summarizing our main results and by outlining further steps which need to be made in order to perform a detailed comparison with the experimental data.

II. THE QUARK HELICITY TMD AND THE POLARIZED DIPOLE AMPLITUDE

A. Review

In [9], we derived the polarized small- x evolution equations for the TMD quark helicity distribution [44],

$$g_{1L}^q(x, k_T^2) = \frac{1}{(2\pi)^3} \frac{1}{2} \sum_{S_L} S_L \int d^2r dr^- e^{ixP^+r^-} e^{-i\vec{k}\cdot\vec{r}} \langle P, S_L | \bar{\psi}(0) \mathcal{U}[0, r] \frac{\gamma^+ \gamma^5}{2} \psi(r) | P, S_L \rangle_{r^+=0}, \quad (5)$$

by relating it to a “polarized dipole amplitude” $G(x_{10}^2, zs)$, giving

$$g_{1L}^{q,S}(x, k_T^2) = \frac{8N_c}{(2\pi)^6} \sum_f \int_{\Lambda^2/s}^1 \frac{dz}{z} \int d^2x_{01} d^2x_{0'1} e^{-i\vec{k}\cdot(\vec{x}_{01}-\vec{x}_{0'1})} \frac{\vec{x}_{01} \cdot \vec{x}_{0'1}}{x_{01}^2 x_{0'1}^2} G(x_{10}^2, zs = \frac{z}{x} Q^2) \quad (6)$$

in the flavor-singlet case [37]. In the above and throughout this paper, we use light-front coordinates $x^\pm \equiv \frac{1}{\sqrt{2}}(x^0 \pm x^3)$, denote transverse vectors (x_\perp^1, x_\perp^2) by \underline{x} and their magnitudes by $x_T \equiv |\underline{x}|$, and indicate differences in transverse coordinates by the abbreviated notation $\underline{x}_{10} \equiv \underline{x}_1 - \underline{x}_0$. The center-of-mass energy squared for the scattering process is s , the infrared (IR) transverse momentum cutoff is Λ , and z is the fraction of the light-cone momentum of the dipole carried by the polarized (anti-)quark. As is well-known, the TMD (5) contains a process-dependent gauge link $\mathcal{U}[0, r]$. For specificity, in [9] we considered semi-inclusive deep inelastic scattering (SIDIS), although the resulting small- x evolution equations also apply to the collinear quark helicity distribution, which is process independent.

The impact-parameter integrated polarized dipole amplitude is

$$G(x_{10}^2, zs) = \int d^2b_{10} G_{10}(zs) \quad (7)$$

with $b_{10} = (\underline{x}_1 + \underline{x}_0)/2$. The polarized dipole scattering amplitude $G_{10}(zs)$ was defined as the polarized generalization of the forward dipole S-matrix in terms of Wilson lines [9]:

$$\begin{aligned} G_{10}(zs) &\equiv \frac{1}{2N_c} \left\langle \left\langle \text{tr} \left[V_0 V_1^{pol\dagger} \right] + \text{tr} \left[V_1^{pol} V_0^\dagger \right] \right\rangle \right\rangle (zs) \\ &\equiv \frac{zs}{2N_c} \left\langle \text{tr} \left[V_0 V_1^{pol\dagger} \right] + \text{tr} \left[V_1^{pol} V_0^\dagger \right] \right\rangle (zs), \end{aligned} \quad (8)$$

where the double-angle brackets are defined to scale out the center-of-mass energy zs between the polarized (anti)quark and the target. While the unpolarized Wilson lines in Eq. (8) are the standard eikonal gauge links (in the fundamental

representation),

$$V_{\underline{0}} \equiv V_{\underline{x}_0}[+\infty, -\infty] \equiv \mathcal{P} \exp \left[ig \int_{-\infty}^{+\infty} dx^- A^+(x^+ = 0, x^-, \underline{x}_0) \right], \quad (9)$$

the polarized Wilson lines $V_{\underline{1}}^{pol}$ are more complex operators. Wilson lines in general correspond to the eikonal propagators of partons in the background field of the target, with the eikonal gauge link (9) being manifestly spin-independent. The polarized Wilson line $V_{\underline{1}}^{pol}$ represents the spin-dependent propagator of a quark in the background field of the target, which in the high-energy limit is suppressed by one factor of the center-of-mass energy, motivating the rescaling performed in Eq. (8). Spin dependence is introduced into the polarized Wilson line by the insertion of exactly one sub-eikonal interaction which is sensitive to the spins of the parton and the target. As discussed in [9], the spin-dependent interaction may correspond either to the t -channel exchange of two quarks or of the transverse component of the gluon field. Because each such sub-eikonal interaction leads to a suppression of the Wilson line by a factor of the energy, additional spin-dependent exchanges can be neglected as power suppressed. While we leave the determination of the quark-exchange part of the polarized Wilson line operator for future work, we will show by explicit calculation below that the gluon-exchange component takes the form

$$(V_{\underline{x}}^{pol})^g = \int_{-\infty}^{+\infty} dx^- V_{\underline{x}}[+\infty, x^-] \hat{\mathcal{O}}_{pol}^g(0^+, x^-, \underline{x}) V_{\underline{x}}[x^-, -\infty] \quad (10)$$

with the effective vertex $\hat{\mathcal{O}}_{pol}^g$ computed in Eq. (17) (see also Eq. (18)). Here we have defined an abbreviated notation for the light-cone Wilson line in the fundamental representation,

$$V_{\underline{x}}[b^-, a^-] = \mathcal{P} \exp \left[ig \int_{a^-}^{b^-} dx^- A^+(x^+ = 0, x^-, \underline{x}) \right]. \quad (11)$$

The small- x limit of the quark helicity distribution (6) corresponds to the large- s limit of the polarized dipole amplitude $G(x_{10}^2, zs)$. The evolution equations for the latter, derived in [9], resum double logarithms of the energy, $\alpha_s \ln^2 \frac{s}{\Lambda^2} \sim \alpha_s \ln^2 \frac{1}{x} \sim 1$. Interestingly, in addition to the “soft logarithm” coming from the longitudinal momentum integral which is also generated by the unpolarized BFKL/BK/JIMWLK evolution, the polarized dipole amplitude is especially sensitive to short-distance fluctuations about the polarized Wilson line, generating an additional logarithm of energy coming from the transverse momentum integration. Preserving these transverse logarithms of energy in the double-logarithmic approximation (DLA) requires imposing a lifetime ordering constraint on the successive steps of evolution, similar to the “kinematical improvements” which become important in the unpolarized evolution at NLO (see, for example, [45]). Like in the unpolarized case, the small- x evolution equations for the polarized dipole amplitude lead to an infinite operator hierarchy, but simplify to a closed set of equations in the large- N_c limit, where N_c is the number of colors. In the large- N_c limit, with DLA accuracy, the polarized evolution equations are [9, 37]

$$G(x_{10}^2, zs) = G^{(0)}(x_{10}^2, zs) + \frac{\alpha_s N_c}{2\pi} \int_{\frac{1}{x_{10}^2 s}}^z \frac{dz'}{z'} \int_{\frac{1}{z' s}}^{x_{10}^2} \frac{dx_{21}^2}{x_{21}^2} [\Gamma(x_{10}^2, x_{21}^2, z' s) + 3G(x_{21}^2, z' s)], \quad (12a)$$

$$\Gamma(x_{10}^2, x_{21}^2, z' s) = G^{(0)}(x_{10}^2, z' s) + \frac{\alpha_s N_c}{2\pi} \int_{\frac{1}{x_{10}^2 s}}^{z'} \frac{dz''}{z''} \int_{\frac{1}{z'' s}}^{\min[x_{10}^2, x_{21}^2 \frac{z'}{z''}]} \frac{dx_{32}^2}{x_{32}^2} [\Gamma(x_{10}^2, x_{32}^2, z'' s) + 3G(x_{32}^2, z'' s)], \quad (12b)$$

where $G^{(0)}$ are the initial conditions. Because of the lifetime ordering condition necessary to preserve the double-logarithmic structure, the polarized dipole G depends upon an auxiliary function Γ , termed the “neighbor dipole amplitude”, in which further evolution is constrained by the lifetime of an adjacent dipole. We also note that, although nonlinear saturation corrections can be incorporated straightforwardly, even at leading order they resum only leading logarithms $\alpha_s \ln \frac{1}{x}$ and are beyond DLA accuracy. As such, the evolution equations (12) are the quark helicity analog of the linear BFKL equation.

Equations (12) were solved numerically in [38] and analytically in [39] for the high-energy asymptotics yielding

$$G(x_{10}^2, zs) = \frac{1}{3} G_0 (zs x_{10}^2)^{\alpha_h^q} \quad (13a)$$

$$\Gamma(x_{10}^2, x_{21}^2, zs) = \frac{1}{3} G_0 (zs x_{21}^2)^{\alpha_h^q} \left[4 \left(\frac{x_{10}^2}{x_{21}^2} \right)^{\frac{\alpha_h^q}{4}} - 3 \right], \quad (13b)$$

where the exponent of the energy, known as the “quark helicity intercept” in analogy to the Pomeron intercept, is given by

$$\alpha_h^q = \frac{4}{\sqrt{3}} \sqrt{\frac{\alpha_s N_c}{2\pi}} \approx 2.31 \sqrt{\frac{\alpha_s N_c}{2\pi}}. \quad (14)$$

The numerical solution of (12) found in [38] possesses two features which are not immediately obvious from the evolution equations (12): a negligible dependence on the initial conditions $G^{(0)}$ and an emergent scaling behavior. The scaling behavior is an observation that for

$$zs > \frac{1}{x_{10}^2} e^{\zeta_0}, \quad \zeta_0 \approx (1 \div 2) \sqrt{\frac{2\pi}{\alpha_s N_c}}, \quad (15)$$

the polarized dipole and neighbor dipole become functions only of the product of the energy and transverse distances, $G(x_{10}^2, zs) = G(zs x_{10}^2)$ and $\Gamma(x_{10}^2, x_{21}^2, zs) = \Gamma(zs x_{10}^2, zs x_{21}^2)$, rather than being dependent on each variable (made dimensionless with the help of the IR cutoff Λ) individually. The coefficient G_0 in Eq. (13) is then the “scaling initial condition” for when this behavior sets in, or, more precisely, the effective value of the inhomogeneous term $G^{(0)}$ at the onset of scaling. In [39], G_0 was set to 1 as irrelevant for the determination of the intercept, but it is useful to keep here for power-counting purposes.

The main purpose of this paper is to extend the analysis summarized above for the quark helicity distribution to the gluon helicity distribution. We will proceed to derive a relation analogous to (6) between the gluon helicity distribution and a polarized dipole operator, derive its large- N_c evolution equations similar to (12) which employ the solution (13), and obtain the gluon helicity intercept analogous to (14).

B. The Gluonic Contribution to the Polarized Wilson Line Operator

Before proceeding to the gluon helicity distribution, it is a useful exercise to construct the operator $\hat{\mathcal{O}}_{pol}^g$ corresponding to t -channel gluon exchange in the polarized Wilson line. This will provide a valuable cross-check of the quark helicity evolution equations (12) at the operator level later on. We will evaluate Eq. (10) directly by computing the polarization-dependent propagator of a quark in the quasi-classical background field of a heavy nucleus. For consistency with Eq. (10), we choose a frame in which the quark is moving in the light-cone minus direction and the target is moving in the plus direction, and we will work in the $A^- = 0$ gauge. The sub-eikonal vertex $\hat{\mathcal{O}}_{pol}^g$ carries polarization information, while all other interactions are eikonal, as illustrated in Fig. 1. As usual, the Fourier transform to the longitudinal coordinate x^- puts the intermediate quark lines between scatterings on mass shell [46, 47].

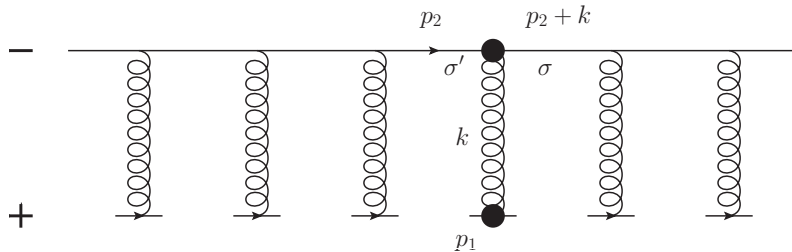


FIG. 1. The polarized Wilson line (10) in the quasi-classical approximation in $A^- = 0$ gauge. The filled circles denote the spin-dependent sub-eikonal scattering.

With the momenta labeled as in Fig. 1, the non-eikonal vertex is straightforward to compute:

$$\sigma \delta_{\sigma, \sigma'} \hat{\mathcal{O}}_{pol}^g(k) \equiv -\frac{1}{2p_2} \bar{u}_\sigma(p_2 + k) \gamma_\perp^i u_{\sigma'}(p_2) ig A_\perp^i(k) = -\frac{i \sigma}{2p_2} \delta_{\sigma \sigma'} \underline{k} \times \underline{A}(k) ig, \quad (16)$$

where we only keep the spin-dependent terms proportional to σ and A_μ denotes the color matrix $A_\mu^a t^a$ with t^a the fundamental generators of $SU(N_c)$. Fourier transforming to coordinate space gives

$$\begin{aligned}\hat{O}_{pol}^g(x^-, \underline{x}) &\equiv \int \frac{dk^+}{2\pi} \frac{d^2k}{(2\pi)^2} e^{-ik^+ x^-} e^{i\vec{k} \cdot \underline{x}} \left[\frac{g}{2p_2^-} \underline{k} \times \underline{A}(k) \right] \\ &= \frac{1}{s} (-igp_1^+) \epsilon_T^{ij} \frac{\partial}{\partial x_\perp^i} A_\perp^j(x^-, \underline{x}) \equiv \frac{1}{s} (-igp_1^+) \underline{\nabla} \times \underline{A}(x^-, \underline{x}),\end{aligned}\quad (17)$$

where $s = 2p_1^+ p_2^-$ is the center-of-mass energy of the polarization-dependent interaction and p_1^+ is the momentum of the polarized nucleon. We have defined $\underline{\nabla} \equiv (\partial/\partial x^1, \partial/\partial x^2)$ and the cross-product $\underline{u} \times \underline{v} = \epsilon_T^{ij} u^i v^j = u^1 v^2 - u^2 v^1$. Here $\epsilon_T^{12} = 1 = -\epsilon_T^{21}$ and $\epsilon_T^{11} = \epsilon_T^{22} = 0$ and Latin indices denote transverse components of 4-vectors, $i, j = 1, 2$. We observe that $\underline{\nabla} \times \underline{A} = -(\partial_\perp^1 A_\perp^2 - \partial_\perp^2 A_\perp^1)$ is the negative of the Abelian part of the field-strength tensor F^{12} . In the $A^- = 0$ gauge we are working in, the non-Abelian contribution $\sim [A_\perp^1, A_\perp^2]$ is further suppressed by an extra $1/s$, but will appear in other gauges. We therefore conclude¹ that the non-eikonal vertex \hat{O}_{pol}^g when expressed in the most-general gauge-covariant form is proportional to the gluon field-strength tensor F^{12} ; we write

$$(V_{\underline{x}}^{pol})^g = \frac{igp_1^+}{s} \int_{-\infty}^{+\infty} dx^- V_{\underline{x}}[+\infty, x^-] F^{12}(x^+ = 0, x^-, \underline{x}) V_{\underline{x}}[x^-, -\infty]. \quad (18)$$

It is also instructive to calculate the spin-dependent field $A_\perp^j(x^-, \underline{x})$ explicitly for a quark target with helicity S_L and momentum p_1^+ , giving

$$A^{aj}(x^-, \underline{x}) = \frac{g}{2\pi} (t^a) S_L \delta_{S_L S_L'} \frac{1}{2p_1^+} \delta(x^-) \epsilon^{ij} \frac{x_\perp^j}{x_\perp^2} \quad (19)$$

for the transverse field entering Eq. (17). The exact form of (19) is specific to the quark target model, but the $1/p^+$ suppression is a general feature of the sub-eikonal spin-dependent exchange. Hence we may write

$$\underline{A}(x^-, \underline{x}) = \frac{S_L}{2p_1^+} \bar{\underline{A}}(x^-, \underline{x}) \quad (20)$$

to scale out the sub-eikonal suppression of the emission vertex in the target and equivalently write the polarized Wilson line as

$$\begin{aligned}(V_{\underline{x}}^{pol})^g &= \frac{1}{2s} \int_{-\infty}^{\infty} dx^- V_{\underline{x}}[+\infty, x^-] \left(-ig \epsilon_T^{ij} \frac{\partial}{\partial x_\perp^i} \bar{A}_\perp^j(x^-, \underline{x}) \right) V_{\underline{x}}[x^-, -\infty] \\ &= \frac{ig}{2s} \int_{-\infty}^{\infty} dx^- V_{\underline{x}}[+\infty, x^-] \bar{F}^{12}(x^-, \underline{x}) V_{\underline{x}}[x^-, -\infty],\end{aligned}\quad (21)$$

where $\bar{F}^{12} = (2p_1^+/S_L) F^{12}$ and all of the energy suppression is contained in the prefactor $1/s$ which is then scaled out in the definition of the polarized dipole amplitude in Eq. (8). We have also put $S_L = +1$, which will be our standard assumption about the helicity of the target from now on, unless specified otherwise by notation.

Employing Eq. (21) in Eq. (8) we can finally write down an explicit operator expression for the polarized dipole scattering amplitude (in $A^- = 0$ gauge):

$$G_{10}(zs) \equiv \frac{p_1^+}{2N_c} \int_{-\infty}^{\infty} dx_1^- \left\langle \text{tr} \left[V_{\underline{0}} V_{\underline{1}}[-\infty, x_1^-] \left(ig \epsilon_T^{ij} \frac{\partial}{\partial (x_1)_\perp^i} A_\perp^j(x_1^-, \underline{x}_1) \right) V_{\underline{1}}[x_1^-, \infty] \right] + \text{c.c.} \right\rangle (zs). \quad (22)$$

¹ We thank Ian Balitsky for this insight.

III. THE GLUON HELICITY TMDs AND NEW POLARIZED DIPOLE AMPLITUDE(S)

The gluon helicity TMD is defined ² similarly to (5) as [51]

$$g_{1L}^G(x, k_T^2) = \frac{-2i}{x P^+} \frac{1}{2} \sum_{S_L} S_L \int \frac{d\xi^- d^2\xi}{(2\pi)^3} e^{ixP^+ \xi^- - i\mathbf{k} \cdot \underline{\xi}} \langle P, S_L | \epsilon_T^{ij} \text{tr} [F^{+i}(0) \mathcal{U}[0, \xi] F^{+j}(\xi) \mathcal{U}'[\xi, 0]] | P, S_L \rangle_{\xi^+=0}. \quad (23)$$

For gluon TMD distributions, the field strength operators are connected by two fundamental gauge links \mathcal{U} , \mathcal{U}' which may separately be either future-pointing ($[+]$) or past-pointing ($[-]$), with

$$\mathcal{U}^{[+]}[y, x] \equiv \mathcal{P} \exp \left[ig \int_{+\infty}^{y^-} dz^- A^+(0^+, z^-, \underline{y}) \right] \mathcal{P} \exp \left[-ig \int_{\underline{x}}^{\underline{y}} d\underline{z} \cdot \underline{A}(0^+, +\infty^-, \underline{z}) \right] \mathcal{P} \exp \left[ig \int_{x^-}^{+\infty} dz^- A^+(0^+, z^-, \underline{x}) \right] \quad (24a)$$

$$\mathcal{U}^{[-]}[y, x] \equiv \mathcal{P} \exp \left[ig \int_{-\infty}^{y^-} dz^- A^+(0^+, z^-, \underline{y}) \right] \mathcal{P} \exp \left[-ig \int_{\underline{x}}^{\underline{y}} d\underline{z} \cdot \underline{A}(0^+, -\infty^-, \underline{z}) \right] \mathcal{P} \exp \left[ig \int_{x^-}^{-\infty} dz^- A^+(0^+, z^-, \underline{x}) \right]. \quad (24b)$$

(The minus sign in the middle exponent in both equations (24) is due to the metric.) Of particular interest are the “dipole distribution” $g_{1L}^{G dip}$ for which one is future pointing and the other is past pointing, $\mathcal{U} = \mathcal{U}^{[+]}$, $\mathcal{U}' = \mathcal{U}^{[-]}$, and the “Weizsäcker-Williams distribution” $g_{1L}^{G WW}$ for which both are future pointing, $\mathcal{U} = \mathcal{U}^{[+]}$, $\mathcal{U}' = \mathcal{U}^{[+]}$.

A. Dipole Gluon Helicity TMD

In this paper we will focus primarily on the “dipole-type” gluon helicity distribution. Starting with Eq. (23) with the appropriate gauge links, we multiply and divide by a volume factor $V^- = \int d^2x dx^-$ and shift the operators in the matrix element to write

$$g_{1L}^{G dip}(x, k_T^2) = \frac{-2i}{x P^+ V^-} \frac{1}{(2\pi)^3} \frac{1}{2} \sum_{S_L} S_L \int d\xi^- d^2\xi d\zeta^- d^2\zeta e^{ixP^+ (\xi^- - \zeta^-)} e^{-i\mathbf{k} \cdot (\underline{\xi} - \underline{\zeta})} \\ \times \langle P, S_L | \epsilon_T^{ij} \text{tr} [F^{+i}(\zeta) \mathcal{U}^{[+]}[\zeta, \xi] F^{+j}(\xi) \mathcal{U}^{[-]}[\xi, \zeta]] | P, S_L \rangle_{\zeta^+=\xi^+=0}. \quad (25)$$

We next convert from the matrix element of a momentum-space eigenstate to a wave packet which is localized in both impact parameter and momentum space:

$$\frac{1}{2P^+ V^-} \langle P, S_L | \cdots | P, S_L \rangle = \int d^2b db^- \rho(b, b^-) \langle p, b, S_L | \cdots | p, b, S_L \rangle \equiv \langle \cdots \rangle_{P, S_L}. \quad (26)$$

This procedure is standard in the color-glass-condensate framework and is used to match the “unintegrated gluon distribution” and the gluon TMD f_1^g in the unpolarized sector [40, 52]; it is also similar to the calculation of the TMDs of a heavy nucleus in the quasi-classical approximation [10]. Applying this to the dipole gluon helicity TMD gives

$$g_{1L}^{G dip}(x, k_T^2) = \frac{-4i}{x} \frac{1}{(2\pi)^3} \int d\xi^- d^2\xi d\zeta^- d^2\zeta e^{ixP^+ (\xi^- - \zeta^-)} e^{-i\mathbf{k} \cdot (\underline{\xi} - \underline{\zeta})} \\ \times \left\langle \epsilon_T^{ij} \text{tr} [F^{+i}(\zeta) \mathcal{U}^{[+]}[\zeta, \xi] F^{+j}(\xi) \mathcal{U}^{[-]}[\xi, \zeta]] \right\rangle, \quad (27)$$

where we have again put $S_L = +1$ for simplicity and dropped the P, S_L subscript off the angle brackets for brevity.

To go further, we need to specify a gauge; we will work in the $A^- = 0$ light-cone gauge, which is equivalent to the covariant gauge in the quasi-classical approximation and is also convenient for including logarithmic small- x evolution. In this gauge, the target field is localized in x^- such that the transverse segments of the staple-shaped gauge links $\mathcal{U}^{[\pm]}$ at $x^- = \pm\infty$ do not contribute, leaving

$$g_{1L}^{G dip}(x, k_T^2) = \frac{-4i}{x} \frac{1}{(2\pi)^3} \int d\xi^- d^2\xi d\zeta^- d^2\zeta e^{ixP^+ (\xi^- - \zeta^-)} e^{-i\mathbf{k} \cdot (\underline{\xi} - \underline{\zeta})} \\ \times \epsilon_T^{ij} \left\langle \text{tr} [V_{\underline{\zeta}}[-\infty, \zeta^-] F^{+i}(\zeta) V_{\underline{\zeta}}[\zeta^-, +\infty] V_{\underline{\xi}}[+\infty, \xi^-] F^{+j}(\xi) V_{\underline{\xi}}[\xi^-, -\infty]] \right\rangle, \quad (28)$$

² Note the differing normalizations and conventions, e.g. Refs. [40, 48–51].

where we have used the cyclicity of the color trace. For the unpolarized gluon distribution, it is sufficient to replace the field-strength tensors by their eikonal approximations, $F^{+i} \approx -\partial_\perp^i A^+$, but since the gluon helicity distribution contains a sub-eikonal contribution, we must expand the product of field-strength tensors to the first non-vanishing sub-eikonal order:

$$F^{+i}(\zeta) \cdots F^{+j}(\xi) = \left(\partial^+ A_\perp^i(\zeta) - \partial^i A^+(\zeta) - ig[A^+(\zeta), A_\perp^i(\zeta)] \right) \cdots \left(\partial^+ A_\perp^j(\xi) - \partial^j A^+(\xi) - ig[A^+(\xi), A_\perp^j(\xi)] \right) \quad (29)$$

$$\approx \left(\frac{\partial}{\partial \zeta^-} A_\perp^i(\zeta) - ig[A^+(\zeta), A_\perp^i(\zeta)] \right) \cdots \left(\frac{\partial}{\partial \xi_\perp^j} A^+(\xi) \right) + \left(\frac{\partial}{\partial \zeta_\perp^i} A^+(\zeta) \right) \cdots \left(\frac{\partial}{\partial \xi^-} A_\perp^j(\xi) - ig[A^+(\xi), A_\perp^j(\xi)] \right).$$

We next convert the sub-eikonal part of the field-strength tensor $F^{+i}(\zeta)$ into a total derivative,

$$V_\zeta[-\infty, \zeta^-] \left(\frac{\partial}{\partial \zeta^-} A_\perp^i(\zeta) - ig[A^+(\zeta), A_\perp^i(\zeta)] \right) V_\zeta[\zeta^-, +\infty] = \frac{\partial}{\partial \zeta^-} \left(V_\zeta[-\infty, \zeta^-] A_\perp^i(\zeta) V_\zeta[\zeta^-, +\infty] \right), \quad (30)$$

which can then be integrated by parts to act on the Fourier factor and generate a net factor of $+ixP^+$. In the same way, the sub-eikonal part of the $F^{+j}(\xi)$ field-strength tensor can be converted into a net factor of $-ixP^+$ and the operator $A_\perp^j(\xi)$. After taking these derivatives, we can safely set $e^{ixP^+(\xi^- - \zeta^-)} \approx 1$ (thus neglecting higher powers of $x \ll 1$), giving

$$g_{1L}^{G dip}(x, k_T^2) = 4P^+ \frac{1}{(2\pi)^3} \int d\xi^- d^2\xi d\zeta^- d^2\zeta e^{-ik \cdot (\xi - \zeta)} \epsilon_T^{ij}$$

$$\times \left\{ \left\langle \text{tr} \left[V_\zeta[-\infty, \zeta^-] A^i(\zeta) V_\zeta[\zeta^-, +\infty] V_\xi[+\infty, \xi^-] \left(\frac{\partial}{\partial \xi_\perp^j} A^+(\xi) \right) V_\xi[\xi^-, -\infty] \right] \right\rangle \right.$$

$$\left. - \left\langle \text{tr} \left[V_\zeta[-\infty, \zeta^-] \left(\frac{\partial}{\partial \zeta_\perp^i} A^+(\zeta) \right) V_\zeta[\zeta^-, +\infty] V_\xi[+\infty, \xi^-] A^j(\xi) V_\xi[\xi^-, -\infty] \right] \right\rangle \right\}. \quad (31)$$

We can now similarly convert the eikonal parts of the field-strength tensors into total derivatives,

$$\int_{-\infty}^{\infty} d\zeta^- V_\zeta[-\infty, \zeta^-] \left(\frac{\partial}{\partial \zeta_\perp^i} A^+(\zeta) \right) V_\zeta[\zeta^-, +\infty] = \frac{i}{g} \frac{\partial}{\partial \zeta_\perp^i} V_\zeta[-\infty, +\infty], \quad (32)$$

which absorbs the $d\zeta^-$ integral from the TMD and can be integrated by parts to generate a net factor of $\frac{1}{g} k_\perp^i$:

$$g_{1L}^{G dip}(x, k_T^2) = \frac{-4}{g(2\pi)^3} P^+ \int d^2\xi d^2\zeta e^{-ik \cdot (\xi - \zeta)} k_\perp^i \epsilon_T^{ij}$$

$$\times \left\{ \left\langle \text{tr} \left[\left(\int d\zeta^- V_\zeta[-\infty, \zeta^-] A^j(\zeta) V_\zeta[\zeta^-, +\infty] \right) V_\xi[+\infty, -\infty] \right] \right\rangle \right.$$

$$\left. + \left\langle \text{tr} \left[V_\zeta[-\infty, +\infty] \left(\int d\xi^- V_\xi[+\infty, \xi^-] A^j(\xi) V_\xi[\xi^-, -\infty] \right) \right] \right\rangle \right\}, \quad (33)$$

where we also swapped $i \leftrightarrow j$ in the first term.

We observe that the sub-eikonal gluon vertex enters in a form similar to Eq. (10), but with an explicit transverse index. Defining the analogous polarized Wilson line (one may call it the polarized Wilson line of the second kind to distinguish it from Eq. (21))

$$(V_\perp^{pol})_\perp^i \equiv \int_{-\infty}^{+\infty} dx^- V_\perp[+\infty, x^-] (ig P^+ A_\perp^i(x)) V_\perp[x^-, -\infty]$$

$$= \frac{1}{2} \int_{-\infty}^{+\infty} dx^- V_\perp[+\infty, x^-] (ig \bar{A}_\perp^i(x)) V_\perp[x^-, -\infty] \quad (34)$$

allows us to write the dipole gluon helicity TMD in a more compact form (compare this with a very similar Eq. (47) in [53])

$$g_{1L}^{G dip}(x, k_T^2) = \frac{-4i}{g^2(2\pi)^3} \int d^2\xi d^2\zeta e^{-ik \cdot (\xi - \zeta)} k_\perp^i \epsilon_T^{ij} \left\{ \left\langle \text{tr} \left[V_\xi (V_\zeta^{pol\dagger})_\perp^j \right] \right\rangle - \left\langle \text{tr} \left[(V_\xi^{pol})_\perp^j V_\zeta^\dagger \right] \right\rangle \right\}, \quad (35)$$

where, for brevity, we have also dropped the explicit integration limits from the infinite unpolarized Wilson lines. Swapping $\underline{\zeta} \leftrightarrow \underline{\xi}$ in the last term generates a minus sign and makes the two terms in braces complex conjugates of one another. Relabeling the dummy integration variables $\underline{\zeta}$ and $\underline{\xi}$ as \underline{x}_1 and \underline{x}_0 , respectively, and changing variables to $d^2x_0 d^2x_1 = d^2x_{10} d^2b_{10}$ with $\underline{b}_{10} \equiv \frac{1}{2}(\underline{x}_1 + \underline{x}_0)$ the impact parameter, we can write

$$g_{1L}^{G dip}(x, k_T^2) = \frac{-4i}{g^2(2\pi)^3} \int d^2x_{10} d^2b_{10} e^{+i\vec{k} \cdot \underline{x}_{10}} k_{\perp}^i \epsilon_T^{ij} \left\{ \left\langle \text{tr} \left[V_{\underline{0}} (V_{\underline{1}}^{pol \dagger})_{\perp}^j \right] \right\rangle + \text{c.c.} \right\}. \quad (36)$$

Defining another dipole-like polarized operator

$$G_{10}^i(zs) \equiv \frac{1}{2N_c} \left\langle \text{tr} \left[V_{\underline{0}} (V_{\underline{1}}^{pol \dagger})_{\perp}^i \right] + \text{c.c.} \right\rangle (zs) \quad (37)$$

we rewrite the dipole gluon helicity TMD as

$$g_{1L}^{G dip}(x, k_T^2) = \frac{-8i N_c}{g^2(2\pi)^3} \int d^2x_{10} e^{i\vec{k} \cdot \underline{x}_{10}} k_{\perp}^i \epsilon_T^{ij} \left[\int d^2b_{10} G_{10}^j(zs = \frac{Q^2}{x}) \right]. \quad (38)$$

The dipole gluon helicity TMD is related to an operator which is, surprisingly, different from the polarized dipole amplitude in Eq. (22). This is very different from the situation with the unpolarized gluon TMDs for which the dipole gluon TMD was related to the (unpolarized adjoint) dipole scattering amplitude on the target proton or nucleus [40]. This relation gave rise to the “dipole” designation of this TMD. Here we see that this relation is not universal and is not valid for the dipole gluon helicity TMD, therefore putting the designation in question as well.

After the integration over all impact parameters, the new polarized dipole amplitude is a vector-valued function of \underline{x}_{10} alone, allowing us to write the decomposition

$$\int d^2b_{10} G_{10}^i(zs) = (x_{10})_{\perp}^i G_1(x_{10}^2, zs) + \epsilon_T^{ij} (x_{10})_{\perp}^j G_2(x_{10}^2, zs). \quad (39)$$

By further writing $(x_{10})_{\perp}^i$ as a derivative $-i \frac{\partial}{\partial k_{\perp}^i}$ on the Fourier factor, we see that the scalar function G_1 does not contribute to the dipole gluon helicity TMD, leaving only

$$\begin{aligned} g_{1L}^{G dip}(x, k_T^2) &= \frac{8i N_c}{g^2(2\pi)^3} \int d^2x_{10} e^{i\vec{k} \cdot \underline{x}_{10}} \underline{k} \cdot \underline{x}_{10} G_2(x_{10}^2, zs = \frac{Q^2}{x}) \\ &= \frac{N_c}{2\pi^4 \alpha_s} k_T^2 \frac{\partial}{\partial k_T^2} \left[\int d^2x_{10} e^{i\vec{k} \cdot \underline{x}_{10}} G_2(x_{10}^2, zs = \frac{Q^2}{x}) \right]. \end{aligned} \quad (40)$$

For future purposes, it is also useful to convert the derivatives back into coordinate space, writing

$$\begin{aligned} g_{1L}^{G dip}(x, k_T^2) &= \frac{1}{\alpha_s 8\pi^4} \int d^2x_0 d^2x_1 e^{i\vec{k} \cdot \underline{x}_{10}} \epsilon_T^{ij} \left\langle \text{tr} \left[(V_{\underline{1}}^{pol})_{\perp}^i \left(\frac{\partial}{\partial (x_0)_{\perp}^j} V_{\underline{0}}^{\dagger} \right) \right] + \text{c.c.} \right\rangle \\ &= \frac{-N_c}{\alpha_s 2\pi^4} \int d^2x_{10} e^{i\vec{k} \cdot \underline{x}_{10}} \left[1 + x_{10}^2 \frac{\partial}{\partial x_{10}^2} \right] G_2(x_{10}^2, zs = \frac{Q^2}{x}). \end{aligned} \quad (41)$$

We have thus expressed the dipole gluon helicity TMD in terms of a polarized dipole operator; Eqs. (40) and (41) should be compared with Eq. (6) from the quark helicity TMD. Unexpectedly, however, the polarized dipole operator (37) which determines the dipole gluon helicity TMD is different from the polarized dipole amplitude (22) which determines the quark helicity TMD. Comparing the underlying polarized Wilson lines, we see that the quark case (21) is sensitive to a *local* derivative $\underline{\nabla} \times \underline{A}(x^-)$ reflecting spin-dependent coupling at some point in the propagation through the target. On the other hand, the gluon case (36) is sensitive to a *total* derivative $\underline{k} \times \underline{V}^{pol} \rightarrow \underline{\nabla} \times \underline{V}^{pol}$ reflecting an overall circular polarization which remains after the entire interaction with the target. In principle, it would seem that quark helicity and gluon helicity are very different quantities, with the gluon helicity requiring not only that a spin-dependent scattering take place but also that the circular-polarized structure survive the rest of the rescattering. We will thus need to derive new evolution equations analogous to Eq. (12) for the new polarized dipole amplitude G_2 in order to determine the small- x asymptotics of the dipole gluon helicity distribution.

B. Weizsäcker-Williams Gluon Helicity TMD

For completeness and further comparison, we will also evaluate the “Weizsäcker-Williams (WW) gluon helicity TMD”:

$$g_{1L}^{GWW}(x, k_T^2) = \frac{-4i}{x} \frac{1}{(2\pi)^3} \int d\xi^- d^2\xi d\zeta^- d^2\zeta e^{ixP^+(\xi^- - \zeta^-)} e^{-ik \cdot (\xi - \zeta)} \times \left\langle \epsilon_T^{ij} \text{tr} \left[F^{+i}(\zeta) \mathcal{U}^{[+]}[\zeta, \xi] F^{+j}(\xi) \mathcal{U}^{[+]}[\xi, \zeta] \right] \right\rangle. \quad (42)$$

Because both gauge links are now future-pointing, it is possible to choose a gauge in which the WW gluon distributions possess a simple partonic interpretation; specifically, we choose the $A^+ = 0$ light-cone (LC) gauge with the $\underline{\nabla} \cdot \underline{A}(x^- = +\infty) = 0$ sub-gauge condition (see [54] for a discussion of the LC gauge and its sub-gauges).³ With this choice, the gauge links are unity on both the light-like segments and on the transverse segments at $x^- = +\infty$ (with the physical content of the gauge links having been encoded in the boundary at $x^- = -\infty$), and we also have $F^{+i} = \partial^+ A_{LC}^i$. Integrating the derivatives by parts in the usual way gives

$$g_{1L}^{GWW}(x, k_T^2) = \frac{-4i}{(2\pi)^3} x(P^+)^2 \int d\xi^- d^2\xi d\zeta^- d^2\zeta e^{ixP^+(\xi^- - \zeta^-)} e^{-ik \cdot (\xi - \zeta)} \left\langle \epsilon_T^{ij} \text{tr} \left[A_{LC}^i(\zeta) A_{LC}^j(\xi) \right] \right\rangle. \quad (43)$$

From here, the rest of the calculation is similar to the standard textbook treatment of the unpolarized WW gluon distribution [47]. We first determine the explicit gauge transformation which achieves the form of Eq. (43) in terms of the fields in the $A^- = 0$ or covariant gauge we have used elsewhere. The desired gauge condition

$$0 = A_{LC}^+ = SA^+S^{-1} - \frac{i}{g}(\partial^+ S)S^{-1}, \quad (44)$$

and sub-gauge condition $\underline{\nabla} \cdot \underline{A}_{LC}(x^- = +\infty) = 0$ [55, 56] are easily seen to be satisfied by the gauge transformation

$$S(x) = \mathcal{P} \exp \left\{ ig \int_{x^-}^{+\infty} dx^- A^+(x^-, \underline{x}) \right\} = V_{\underline{x}}[+\infty, x^-]. \quad (45)$$

The transverse components A_{LC}^i we need are given by

$$A_{LC}^i = SA_{\perp}^i S^{-1} - \frac{i}{g}(\partial^i S)S^{-1}, \quad (46)$$

where in the eikonal approximation we would normally neglect the first term compared to the second term on the right-hand side. But for the gluon helicity, we must keep the first sub-eikonal polarization-dependent correction to the product of the two fields, which enters Eq. (46) through A_{\perp}^i :

$$A_{LC}^i(\zeta) A_{LC}^j(\xi) \approx \frac{i}{g} \left(V_{\underline{\zeta}}[+\infty, \zeta^-] A_{\perp}^i(\zeta) V_{\underline{\zeta}}[\zeta^-, +\infty] \right) \left(\frac{\partial}{\partial \xi_{\perp}^j} V_{\underline{\xi}}[+\infty, \xi^-] \right) V_{\underline{\xi}}[\xi^-, +\infty] \\ + \frac{i}{g} \left(\frac{\partial}{\partial \zeta_{\perp}^i} V_{\underline{\zeta}}[+\infty, \zeta^-] \right) V_{\underline{\zeta}}[\zeta^-, +\infty] \left(V_{\underline{\xi}}[+\infty, \xi^-] A_{\perp}^j(\xi) V_{\underline{\xi}}[\xi^-, +\infty] \right). \quad (47)$$

In the small- x limit, the longitudinal coordinate integrals are

$$\int_{-\infty}^{\infty} d\zeta^- e^{ixP^+\zeta^-} V_{\underline{\zeta}}[+\infty, \zeta^-] A_{\perp}^i(\zeta) V_{\underline{\zeta}}[\zeta^-, +\infty] \approx \int_{-\infty}^{\infty} d\zeta^- V_{\underline{\zeta}}[+\infty, \zeta^-] A_{\perp}^i(\zeta) V_{\underline{\zeta}}[\zeta^-, +\infty] \\ = \frac{-i}{gP^+} (V_{\underline{\zeta}}^{pol})_{\perp}^i V_{\underline{\zeta}}^{\dagger} = \frac{i}{gP^+} V_{\underline{\zeta}} (V_{\underline{\zeta}}^{pol\dagger})_{\perp}^i \quad (48)$$

³ Throughout this subsection, we denote the fields in the $A^+ = 0$, $\underline{\nabla} \cdot \underline{A}(x^- = +\infty) = 0$ gauge with the explicit subscript “LC”; fields without explicit subscripts correspond to the $A^- = 0$ gauge used elsewhere in this paper.

and

$$\begin{aligned}
\int_{-\infty}^{\infty} d\xi^- e^{ixP^+\xi^-} \left(\frac{\partial}{\partial \xi_{\perp}^j} V_{\underline{\xi}}[+\infty, \xi^-] \right) V_{\underline{\xi}}[\xi^-, +\infty] &= \\
&= \int_{-\infty}^{+\infty} d\xi^- e^{ixP^+\xi^-} \int_{\xi^-}^{+\infty} dz^- V_{\underline{\xi}}[+\infty, z^-] \left(ig \frac{\partial}{\partial \xi_{\perp}^j} A^+(0^+, z^-, \underline{\xi}) \right) V_{\underline{\xi}}[z^-, +\infty] \\
&= \int_{-\infty}^{+\infty} dz^- \left[\int_{-\infty}^{z^-} d\xi^- e^{ixP^+\xi^-} \right] V_{\underline{\xi}}[+\infty, z^-] \left(ig \frac{\partial}{\partial \xi_{\perp}^j} A^+(0^+, z^-, \underline{\xi}) \right) V_{\underline{\xi}}[z^-, +\infty] \\
&\approx \frac{-i}{xP^+} \int_{-\infty}^{+\infty} dz^- V_{\underline{\xi}}[+\infty, z^-] \left(ig \frac{\partial}{\partial \xi_{\perp}^j} A^+(0^+, z^-, \underline{\xi}) \right) V_{\underline{\xi}}[z^-, +\infty] \\
&= \frac{-i}{xP^+} \left(\frac{\partial}{\partial \xi_{\perp}^j} V_{\underline{\xi}} \right) V_{\underline{\xi}}^{\dagger} = \frac{+i}{xP^+} V_{\underline{\xi}} \left(\frac{\partial}{\partial \xi_{\perp}^j} V_{\underline{\xi}}^{\dagger} \right), \tag{49}
\end{aligned}$$

where we have expanded the exponent to the first non-vanishing term. Inserting all of these expressions into Eq. (43) gives

$$\begin{aligned}
g_{1L}^{GWW}(x, k_T^2) &= \frac{4}{g^2(2\pi)^3} \int d^2\xi d^2\zeta e^{-ik_{\perp} \cdot (\xi - \zeta)} \epsilon_T^{ij} \\
&\quad \times \left\langle \text{tr} \left[(V_{\underline{\zeta}}^{pol})_{\perp}^i V_{\underline{\zeta}}^{\dagger} V_{\underline{\xi}} \left(\frac{\partial}{\partial \xi_{\perp}^j} V_{\underline{\xi}}^{\dagger} \right) \right] - \text{tr} \left[\left(\frac{\partial}{\partial \zeta_{\perp}^i} V_{\underline{\zeta}} \right) V_{\underline{\zeta}}^{\dagger} V_{\underline{\xi}} (V_{\underline{\xi}}^{pol\dagger})_{\perp}^j \right] \right\rangle. \tag{50}
\end{aligned}$$

Swapping $\underline{\zeta} \leftrightarrow \underline{\xi}$ and $i \leftrightarrow j$ in the second term makes it the complex conjugate of the first term. Relabeling the dummy integration variables $\underline{\zeta}$ and $\underline{\xi}$ as \underline{x}_1 and \underline{x}_0 , respectively, and changing variables to $d^2x_0 d^2x_1 = d^2x_{10} d^2b_{10}$ with $b_{10} = \frac{1}{2}(\underline{x}_1 + \underline{x}_0)$ the impact parameter, we can write

$$g_{1L}^{GWW}(x, k_T^2) = \frac{4}{g^2(2\pi)^3} \int d^2x_{10} d^2b_{10} e^{ik_{\perp} \cdot \underline{x}_{10}} \epsilon_T^{ij} \left\langle \text{tr} \left[(V_{\underline{x}_1}^{pol})_{\perp}^i V_{\underline{x}_1}^{\dagger} V_{\underline{x}_0} \left(\frac{\partial}{\partial (x_0)_{\perp}^j} V_{\underline{x}_0}^{\dagger} \right) \right] + \text{c.c.} \right\rangle. \tag{51}$$

It seems that the WW gluon helicity TMD is determined by yet another polarized dipole-like operator

$$G_{10}^{ji}(zs) \equiv \frac{-1}{2N_c} \left\langle \text{tr} \left[(V_{\underline{x}_1}^{pol})_{\perp}^i V_{\underline{x}_1}^{\dagger} V_{\underline{x}_0} \left(\frac{\partial}{\partial (x_0)_{\perp}^j} V_{\underline{x}_0}^{\dagger} \right) \right] + \text{c.c.} \right\rangle (zs) \tag{52}$$

which is a rank-2 tensor in the transverse plane. After integration over impact parameters, we can correspondingly define a scalar function

$$\begin{aligned}
G_3(x_{10}^2, zs) &\equiv \int d^2b_{10} \epsilon_T^{ij} G_{10}^{ji}(zs) \\
&= \frac{-1}{2N_c} \int d^2b_{10} \epsilon_T^{ij} \left\langle \text{tr} \left[(V_{\underline{x}_1}^{pol})_{\perp}^i V_{\underline{x}_1}^{\dagger} V_{\underline{x}_0} \left(\frac{\partial}{\partial (x_0)_{\perp}^j} V_{\underline{x}_0}^{\dagger} \right) \right] + \text{c.c.} \right\rangle (zs) \tag{53}
\end{aligned}$$

in terms of which the WW gluon helicity TMD is written

$$g_{1L}^{GWW}(x, k_T^2) = \frac{-N_c}{4\pi^4 \alpha_s} \int d^2x_{10} e^{ik_{\perp} \cdot \underline{x}_{10}} G_3(x_{10}^2, zs = \frac{Q^2}{x}). \tag{54}$$

We have now expressed the Weizsäcker-Williams gluon helicity TMD as well in terms of a yet another new polarized dipole operator; Eq. (54) for the WW gluon helicity distribution is directly comparable to Eq. (40) for the dipole gluon helicity distribution and Eq. (6) for the quark helicity distribution. The polarized dipole operator (52) for the WW gluon helicity distribution is different still from both the operator (37) for the dipole gluon helicity distribution and the amplitude (22) for the quark helicity distribution. Although the WW gluon helicity distribution is built from the same polarized Wilson line (34) as the dipole gluon helicity distribution, it is incorporated into a more complicated operator due to the future-pointing structure of the WW gauge links: this feature is similar to the unpolarized WW gluon TMD, which is related to the color quadrupole operator instead of a dipole [40, 42].

IV. OPERATOR EVOLUTION EQUATIONS AT SMALL x

Having constructed the appropriate polarized dipole amplitudes for the dipole gluon helicity distribution (37) and Weizsäcker-Williams gluon helicity distribution (52), we will now proceed to derive small- x evolution equations, focusing on the dipole distribution. We will do this at the operator level using a procedure which is similar in spirit (although different in gauge) to the background field method employed in [11].

Beginning with the operator definitions of the polarized Wilson lines and dipole amplitudes, we will separate the gauge fields A^μ of the target into “classical” fields A_{cl}^μ and “quantum” fields a^μ :

$$A^\mu(x) = A_{cl}^\mu(x) + a^\mu(x). \quad (55)$$

This separation can be done using a rapidity regulator η , such that the “fast” quantum fields have rapidities greater than η , while the “slow” classical fields have rapidities less than η and are effectively frozen from the point of view of the quantum fluctuations. (Here “greater” and “smaller” rapidities depend on the choice of a coordinate system, and may be interchanged.) This is essentially the rapidity factorization approach used in [57], and the evolution equations we will derive can be understood as renormalization group equations in the rapidity cutoff η . The classical fields of the target, being enhanced by the target density, will be resummed to all orders. These classical fields (in the $A^- = 0$ light-cone gauge) are localized in x^- to a parametrically small window, which we choose to be centered on the origin: $x^- \in [-R^-, +R^-] \sim [-\frac{1}{p^+}, +\frac{1}{p^+}]$, with p^+ the large momentum of the target. Although the classical fields are Lorentz-contracted to a delta function at $x^- = 0$, the quantum fields can extend far beyond the target; we will calculate the first correction due to these quantum fields in perturbation theory.

As a warm-up exercise and as a cross-check of our previous work [9], we will first employ this method to rederive the evolution equations for the polarized dipole amplitude (8) (or (22)) which governs the quark helicity distribution at small x . We will then repeat this exercise to derive new evolution equations for the polarized dipole amplitude (37) which governs the dipole gluon helicity distribution. We leave the corresponding evolution equations for the Weizsäcker-Williams gluon helicity distribution for future work, although we note that the small- x asymptotics of both gluon helicity distributions must coincide.

A. Evolution of the Polarized Dipole Operator For Quark Helicity

We begin with the polarized dipole amplitude for the quark helicity distribution Eq. (8), using the explicit operator form (21) for the polarized Wilson line (cf. Eq. (22)):

$$G_{10}(zs) \equiv \frac{p^+}{2N_c} \int_{-\infty}^{\infty} dx_1^- \left\langle \text{tr} \left[V_0 V_1[-\infty, x_1^-] \left(ig \epsilon_T^{ij} \frac{\partial}{\partial (x_1)_\perp^i} A_\perp^j(x_1^-, \underline{x}_1) \right) V_1[x_1^-, \infty] \right] + \text{c.c.} \right\rangle (zs). \quad (56)$$

Because this operator contains only t -channel gluon exchange, it will not couple directly to soft quarks. This procedure will therefore only test the gluon emission sector of the quark helicity evolution equations, but this is precisely what is needed to verify the evolution equations in the large- N_c limit.

As in Eq. (55), we first expand the gauge fields into classical and quantum components, both in the Wilson lines and in the explicit operator insertion. We then keep the first quantum correction to the classical background by contracting two of the quantum fields to form a quantum propagator in the background of the classical fields.⁴ We may distinguish the following classes of contractions shown diagrammatically in Fig. 2: “polarized ladder” emissions (I and I’) in which a polarized gluon is emitted and absorbed by line 1; “polarized non-ladder” emissions (II and II’) in which a polarized gluon is exchanged between lines 1 and 0; and unpolarized gluon emissions (dubbed “eikonal” in

⁴ One may note a subtlety of this procedure: strictly, the fields must be time-ordered in order to apply Wick’s theorem and form contractions. The fields entering the operators here are not time-ordered but rather all sit at $x^+ = 0$, which plays the role of time in light-front quantization. Time ordering may be achieved by inserting a complete set of “out” states, as in [40], although the resulting Schwinger-Keldysh ordering is still different from the forward-scattering time ordering implicit in the background field method. The equivalence between these two time-ordered structures was verified in [58] up to next-to-leading order, which is more than sufficient precision for our purposes here.

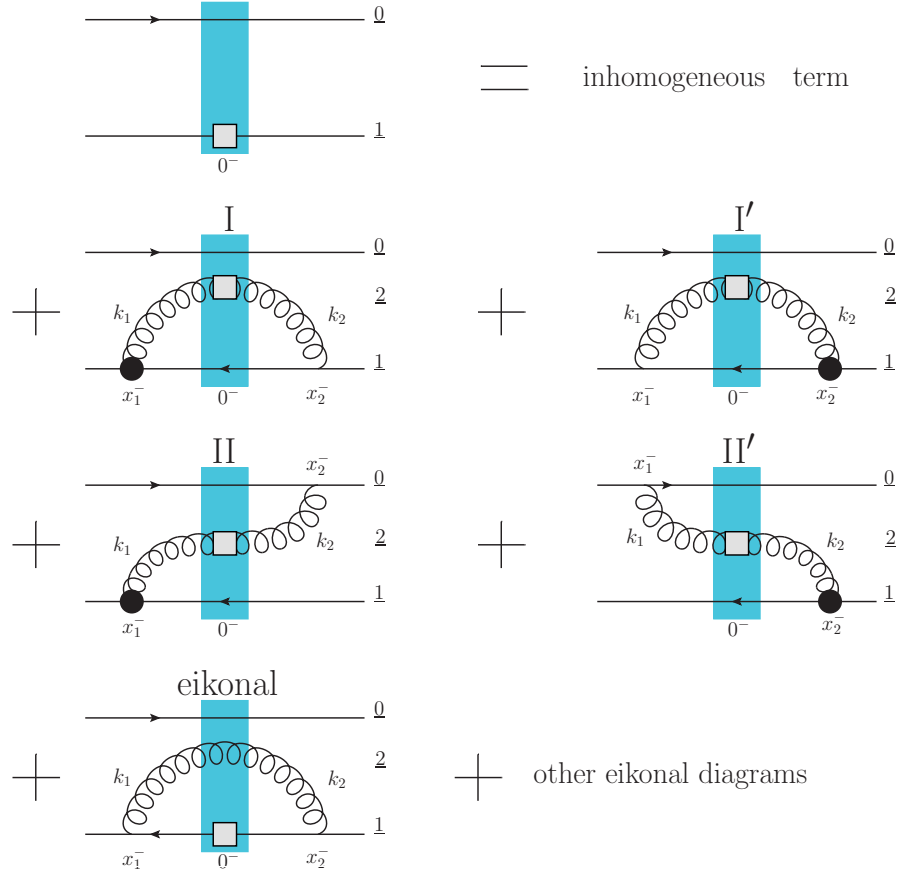


FIG. 2. Diagrams illustrating contractions (57) contributing to the evolution of the polarized dipole amplitude (56) for the quark helicity distribution. The blue band represents the classical fields (shock wave), the black vertex represents the sub-eikonal operator insertion (17), and the gray box represents the polarized Wilson line.

Fig. 2). As visualized in Fig. 2, these contractions are

$$\text{I} : \quad \text{tr} \left[V_{\underline{0}} V_{\underline{1}}[-\infty, x_1^-] \underline{\nabla} \times \overline{a(x_1^-, x_1)} V_{\underline{1}}[x_1^-, \infty] \right] \quad (57a)$$

$$\text{I}' : \quad \text{tr} \left[V_{\underline{0}} \overline{V_{\underline{1}}[-\infty, x_1^-] \underline{\nabla} \times a(x_1^-, x_1)} V_{\underline{1}}[x_1^-, \infty] \right] \quad (57b)$$

$$\text{II} + \text{II}' : \quad \text{tr} \left[\overline{V_{\underline{0}} V_{\underline{1}}[-\infty, x_1^-] \underline{\nabla} \times a(x_1^-, x_1)} V_{\underline{1}}[x_1^-, \infty] \right] \quad (57c)$$

$$\begin{aligned} \text{eikonal} : \quad & \text{tr} \left[V_{\underline{0}} V_{\underline{1}}[-\infty, x_1^-] \underline{\nabla} \times \hat{A}_{cl}(x_1^-, x_1) V_{\underline{1}}[x_1^-, \infty] \right] \\ & + \text{tr} \left[\overline{V_{\underline{0}} V_{\underline{1}}[-\infty, x_1^-] \underline{\nabla} \times \hat{A}_{cl}(x_1^-, x_1)} V_{\underline{1}}[x_1^-, \infty] \right] \\ & + \text{tr} \left[\overline{V_{\underline{0}} V_{\underline{1}}[-\infty, x_1^-] \underline{\nabla} \times \hat{A}_{cl}(x_1^-, x_1)} V_{\underline{1}}[x_1^-, \infty] \right] \\ & + \text{tr} \left[V_{\underline{0}} \overline{V_{\underline{1}}[-\infty, x_1^-] \underline{\nabla} \times \hat{A}_{cl}(x_1^-, x_1)} V_{\underline{1}}[x_1^-, \infty] \right] \\ & + \text{tr} \left[V_{\underline{0}} V_{\underline{1}}[-\infty, x_1^-] \underline{\nabla} \times \hat{A}_{cl}(x_1^-, x_1) \overline{V_{\underline{1}}[x_1^-, \infty]} \right] \\ & + \text{tr} \left[V_{\underline{0}} V_{\underline{1}}[-\infty, x_1^-] \underline{\nabla} \times \hat{A}_{cl}(x_1^-, x_1) \overline{V_{\underline{1}}[x_1^-, \infty]} \right]. \end{aligned} \quad (57d)$$

Consider first the contraction I. Expanding the Wilson line $V_{\underline{1}}[x_1^-, \infty]$ to first order in the quantum field, we have

$$(\delta G_{10})_{\text{I}} = \frac{g^2 p^+}{2N_c} \int_{-\infty}^0 dx_1^- \int_0^\infty dx_2^- \left\langle \text{tr} \left[V_{\underline{0}} t^a V_{\underline{1}}^\dagger t^b \right] \left(\frac{\partial}{\partial (x_1)_\perp^i} \epsilon_T^{ij} a_\perp^{ja}(x_1^-, x_1) \right) a^{+b}(x_2^-, x_1) + \text{c.c.} \right\rangle. \quad (58)$$

After forming the contraction of these two quantum fields, we set $a^\mu = 0$ in the rest of the Wilson lines, such that only the classical background fields contribute. Since these classical fields are localized at $x^- = 0$ we replace the remaining semi-infinite Wilson lines by the fully infinite ones: this is in accordance with the standard calculation in the shock wave background [11]. The contraction between the operator insertion a_\perp^{ja} and the semi-infinite Wilson line $V_{\underline{1}}[x_1^-, \infty]$ explicitly requires $x_2^- > x_1^-$, but in principle there are contributions from $x_1^- < x_2^- < 0$ and $0 < x_1^- < x_2^-$ in addition to the $x_1^- < 0 < x_2^-$ written here. We neglect these sub-eikonal virtual diagrams, since then the antiquark would again need to scatter in the classical field in a spin-dependent way, making them further energy suppressed. Thus only the $x_1^- < 0 < x_2^-$ “real” diagram shown in Fig. 2 contributes. Similarly, only the diagram in which the radiated gluon scatters in a spin-dependent way is capable of receiving logarithmic enhancement at small x .

The contraction in Eq. (58) is the gluon propagator from the sub-eikonal emission vertex to the Wilson line in the background of the classical fields. In general, we can write it as a free propagator from the emission vertex to the shock wave, a Wilson line for the interaction with the shock wave, and another free propagator to the absorption vertex:

$$\begin{aligned} & \int_{-\infty}^0 dx_1^- \int_0^\infty dx_2^- \epsilon_T^{ij} \left(\frac{\partial}{\partial (x_1)_\perp^i} a_\perp^{ja}(x_1^-, x_1) \right) a^{+b}(x_2^-, x_1) = \\ & = \int d^2 x_2 \left[\epsilon_T^{ij} \frac{\partial}{\partial (x_1)_\perp^i} \int_{-\infty}^0 dx_1^- \int \frac{d^4 k_1}{(2\pi)^4} e^{ik_1^+ x_1^-} e^{ik_1 \cdot x_{21}} \frac{-i}{k_1^2 + i\epsilon} N^{j\mu}(k_1) \right] \\ & \quad \times \left[(U_{\underline{2}}^{ba})_{\mu\nu} (2k_1^-) 2\pi \delta(k_1^- - k_2^-) \right] \\ & \quad \times \left[\int_0^\infty dx_2^- \int \frac{d^4 k_2}{(2\pi)^4} e^{-ik_2^+ x_2^-} e^{-ik_2 \cdot x_{21}} \frac{-i}{k_2^2 + i\epsilon} N^{\nu+}(k_2) \right]. \end{aligned} \quad (59)$$

Here the numerator of the free gluon propagator in the $\eta \cdot A \equiv A^- = 0$ light-cone gauge is

$$N^{\mu\nu}(k) = g^{\mu\nu} - \frac{\eta^\mu k^\nu + k^\mu \eta^\nu}{k^-} = - \sum_{\lambda=\pm} (\epsilon_\lambda^*(k))^\mu (\epsilon_\lambda(k))^\nu - \frac{k^2}{(k^-)^2} \eta^\mu \eta^\nu. \quad (60)$$

The contribution from the instantaneous gluon term (last term on the right-hand side of Eq. (60)) is proportional to a delta function in x^- and cannot propagate across the classical shockwave; it therefore does not contribute to real gluon emission. This allows us to replace the numerators by polarization sums and write the interaction with the shockwave as a polarization matrix:

$$(\epsilon_\lambda(k_1))_\mu (U_{\underline{x}}^{ba})^{\mu\nu} (\epsilon_{\lambda'}^*(k_2))_\nu = \delta_{\lambda\lambda'} (U_{\underline{x}})^{ba} + \lambda \delta_{\lambda\lambda'} (U_{\underline{x}}^{pol})^{ba} + \dots, \quad (61)$$

where the ellipsis represents sub-eikonal terms which do not contribute to helicity evolution.

This gives

$$\begin{aligned} \int_{-\infty}^0 dx_1^- \int_0^\infty dx_2^- \epsilon_T^{ij} \left(\frac{\partial}{\partial (x_1)_\perp^i} a_\perp^{ja}(x_1^-, \underline{x}_1) \right) a^{+b}(x_2^-, \underline{x}_1) = \\ = \sum_\lambda \lambda \int d^2 x_2 \left[\epsilon_T^{ij} \frac{\partial}{\partial (x_1)_\perp^i} \int_{-\infty}^0 dx_1^- \int \frac{d^4 k_1}{(2\pi)^4} e^{ik_1^+ x_1^-} e^{ik_1 \cdot \underline{x}_{21}} \frac{-i}{k_1^2 + i\epsilon} (\epsilon_\lambda^*)^j_\perp \right] \\ \times \left[(U_{\underline{x}}^{pol})^{ba} 2\pi(2k_1^-) \delta(k_1^- - k_2^-) \right] \\ \times \left[\int_0^\infty dx_2^- \int \frac{d^4 k_2}{(2\pi)^4} e^{-ik_2^+ x_2^-} e^{-ik_2 \cdot \underline{x}_{21}} \frac{-i}{k_2^2 + i\epsilon} [\epsilon_\lambda(k_2)]^+_\perp \right]. \end{aligned} \quad (62)$$

Each factor in brackets now has a transparent interpretation as the emission vertex of a gluon with physical polarization λ , the polarized Wilson line for that gluon to scatter in the classical field, and the absorption vertex. Performing the spin sum gives $\sum_\lambda \lambda (\epsilon_\lambda^*)^j_\perp [\epsilon_\lambda(k_2)]^+_\perp = i \epsilon_T^{j\ell}(k_2)_\perp^\ell / k_2^-$ (equivalently, we could have just kept the appropriate terms in the numerators (60)), such that

$$\begin{aligned} \int_{-\infty}^0 dx_1^- \int_0^\infty dx_2^- \epsilon_T^{ij} \left(\frac{\partial}{\partial (x_1)_\perp^i} a_\perp^{ja}(x_1^-, \underline{x}_1) \right) a^{+b}(x_2^-, \underline{x}_1) = \\ = \frac{i}{\pi} \int_{-\infty}^\infty dk^- \int d^2 x_2 \left[\frac{\partial}{\partial (x_1)_\perp^i} \int_{-\infty}^0 dx_1^- \int \frac{d^2 k_1 dk_1^+}{(2\pi)^3} e^{ik_1^+ x_1^-} e^{ik_1 \cdot \underline{x}_{21}} \frac{1}{k_1^2 + i\epsilon} \right] \\ \times \left[\int_0^\infty dx_2^- \int \frac{d^2 k_2 dk_2^+}{(2\pi)^3} e^{-ik_2^+ x_2^-} e^{-ik_2 \cdot \underline{x}_{21}} \frac{1}{k_2^2 + i\epsilon} (k_2)_\perp^i \right] (U_{\underline{x}}^{pol})_{(k^-)}^{ba} \Big|_{k_1^- = k_2^- = k^-}. \end{aligned} \quad (63)$$

The integrals in brackets are straightforward to perform:

$$\int_{-\infty}^0 dx_1^- \int \frac{d^2 k_1 dk_1^+}{(2\pi)^3} e^{ik_1^+ x_1^-} e^{ik_1 \cdot \underline{x}_{21}} \frac{1}{k_1^2 + i\epsilon} = \frac{-1}{2\pi} \ln \frac{1}{x_{21}\Lambda} \theta(k_1^-) \quad (64a)$$

$$\frac{\partial}{\partial (x_1)_\perp^i} \left[\frac{-1}{2\pi} \ln \frac{1}{x_{21}\Lambda} \right] = \frac{-1}{2\pi} \frac{(x_{21})_\perp^i}{x_{21}^2} \quad (64b)$$

$$\int_0^\infty dx_2^- \int \frac{d^2 k_2 dk_2^+}{(2\pi)^3} e^{-ik_2^+ x_2^-} e^{-ik_2 \cdot \underline{x}_{21}} \frac{1}{k_2^2 + i\epsilon} (k_2)_\perp^i = \frac{i}{2\pi} \frac{(x_{21})_\perp^i}{x_{21}^2} \theta(k_2^-), \quad (64c)$$

such that the full propagator for contraction I is

$$\int_{-\infty}^0 dx_1^- \int_0^\infty dx_2^- \left(\frac{\partial}{\partial (x_1)_\perp^i} \epsilon_T^{ij} a_\perp^{ja}(x_1^-, \underline{x}_1) \right) a^{+b}(x_2^-, \underline{x}_1) = \frac{1}{4\pi^3} \int_0^\infty dk^- \int \frac{d^2 x_2}{x_{21}^2} (U_{\underline{x}}^{pol})_{(k^-)}^{ba}. \quad (65)$$

The propagator (65) is the backbone of the calculation, trivially giving for diagram I

$$\begin{aligned}
(\delta G_{10})_I(zs) &= \frac{g^2 p^+}{8\pi^3 N_c} \int_0^\infty dk^- \int \frac{d^2 x_2}{x_{21}^2} \left\langle \text{tr} \left[V_0 t^a V_1^\dagger t^b \right] (U_2^{pol})^{ba} + \text{c.c.} \right\rangle (z's = 2p^+ k^-) \\
&= \frac{\alpha_s N_c}{4\pi^2} \int_{\frac{\Lambda^2}{s}}^z \frac{dz'}{z'} \int \frac{d^2 x_2}{x_{21}^2} \left\langle \frac{1}{N_c^2} \text{tr} \left[V_0 t^a V_1^\dagger t^b \right] (U_2^{pol})^{ba} + \text{c.c.} \right\rangle (z's),
\end{aligned} \tag{66}$$

where we have used the double-angle brackets defined in Eq. (8). In the second line of Eq. (66) we have also modified the limits of k^- integration to make sure that k^- does not exceed the large p^- momentum of the projectile in the actual diagrammatic calculation.

It is straightforward to show that the propagators are symmetric, such that diagrams I and I' are equal and diagrams II and II' are equal. In the case of diagram II, the only difference is that the momenta are conjugate to different coordinates on opposite sides of the shock wave (note that a^+ in the contraction is now evaluated at \underline{x}_0):

$$\int_{-\infty}^0 dx_1^- \int_0^\infty dx_2^- \left(\frac{\partial}{\partial (x_1)_\perp^i} \epsilon_T^{ij} a_\perp^{ja}(\underline{x}_1^-, \underline{x}_1) \right) a^{+b}(\underline{x}_2^-, \underline{x}_0) = \frac{1}{4\pi^3} \int_0^\infty dk^- \int d^2 x_2 \frac{x_{21} \cdot x_{20}}{x_{21}^2 x_{20}^2} (U_2^{pol})_{(k^-)}^{ba}, \tag{67}$$

which reduces back to (65) in the limit $\underline{x}_0 \rightarrow \underline{x}_1$. This gives for diagram II

$$\begin{aligned}
(\delta G_{10})_{II}(zs) &\equiv \frac{-g^2 p^+}{2N_c} \int_{-\infty}^0 dx_1^- \int_0^\infty dx_2^- \left\langle \text{tr} \left[V_0 t^a V_1^\dagger t^b \right] \left(\frac{\partial}{\partial (x_1)_\perp^i} \epsilon_T^{ij} a_\perp^{ja}(\underline{x}_1^-, \underline{x}_1) \right) a^{+b}(\underline{x}_2^-, \underline{x}_0) + \text{c.c.} \right\rangle \\
&= -\frac{\alpha_s N_c}{4\pi^2} \int_{\frac{\Lambda^2}{s}}^z \frac{dz'}{z'} \int d^2 x_2 \frac{x_{21} \cdot x_{20}}{x_{21}^2 x_{20}^2} \left\langle \frac{1}{N_c^2} \text{tr} \left[V_0 t^a V_1^\dagger t^b \right] (U_2^{pol})^{ba} + \text{c.c.} \right\rangle (z's).
\end{aligned} \tag{68}$$

The extra minus sign from diagram II comes from having expanded V_0 rather than V_1^\dagger ; that is, from the opposite charge ($-g$) of the antiquark.

The last ingredient in the evolution is the unpolarized eikonal contribution, which can simply be read off of the literature; the only difference is that line 1 for us is polarized.

$$(\delta G_{10})_{\text{eik}}(zs) = \frac{\alpha_s N_c}{2\pi^2} \int_{\frac{\Lambda^2}{s}}^z \frac{dz'}{z'} \int d^2 x_2 \frac{x_{10}^2}{x_{21}^2 x_{20}^2} \left\langle \frac{1}{N_c^2} \text{tr} \left[V_0 t^a V_1^{pol \dagger} t^b \right] (U_2)^{ba} - \frac{C_F}{N_c^2} \text{tr} \left[V_0 V_1^{pol \dagger} \right] + \text{c.c.} \right\rangle (z's). \tag{69}$$

With all three contributions from polarized ladder gluons (I + I', (66)), polarized non-ladder gluons (II + II', (68)), and unpolarized gluons (eikonal, (69)), the complete evolution of the polarized dipole amplitude for the quark helicity distribution is

$$\begin{aligned}
G_{10}(zs) &= G_{10}^{(0)}(zs) + 2(\delta G_{10})_I(zs) + 2(\delta G_{10})_{II}(zs) + (\delta G_{10})_{\text{eik}}(zs) \\
&= G_{10}^{(0)}(zs) + \frac{\alpha_s N_c}{2\pi^2} \int_{\frac{\Lambda^2}{s}}^z \frac{dz'}{z'} \int d^2 x_2 \left\{ \left[\frac{1}{x_{21}^2} - \frac{x_{21} \cdot x_{20}}{x_{21}^2 x_{20}^2} \right] \left\langle \frac{1}{N_c^2} \text{tr} \left[V_0 t^a V_1^\dagger t^b \right] (U_2^{pol})^{ba} + \text{c.c.} \right\rangle (z's) \right. \\
&\quad \left. + \frac{x_{10}^2}{x_{21}^2 x_{20}^2} \left\langle \frac{1}{N_c^2} \text{tr} \left[V_0 t^a V_1^{pol \dagger} t^b \right] (U_2)^{ba} - \frac{C_F}{N_c^2} \text{tr} \left[V_0 V_1^{pol \dagger} \right] + \text{c.c.} \right\rangle (z's) \right\},
\end{aligned} \tag{70}$$

in complete agreement with Eq. (50) of [9]. We should note that the limits of the x_2 integral in each term are set by enforcing a lifetime ordering condition: the lifetime of the quantum fluctuation should be much longer than the subsequent classical interactions, in accordance with the rapidity factorization scheme. The fact that we have successfully re-derived the evolution equation (70) for the polarized dipole amplitude serves as an independent check of Eq. (50) in [9]. It also validates both the operator definition (21) of the polarized Wilson line and our implementation of the operator-level evolution using the background field / rapidity factorization methods. We will next repeat this analysis for the new polarized dipole amplitude (37) for the dipole gluon helicity distribution.

Before we do that, let us make the connection between Eq. (70) and Eqs. (12). Reinstating the lifetime ordering condition on the x_2 integration in the first term in the curly brackets of Eq. (70) multiplies $1/x_{21}^2$ by $\theta(x_{10}^2 z - x_{21}^2 z')$ while multiplying $(x_{21} \cdot x_{20})/(x_{21}^2 x_{20}^2)$ by $\theta(x_{10}^2 z - \max\{x_{21}^2, x_{20}^2\} z')$. The DLA limit of the resulting kernel is obtained by the following substitution:

$$\frac{1}{x_{21}^2} \theta(x_{10}^2 z - x_{21}^2 z') - \frac{x_{21} \cdot x_{20}}{x_{21}^2 x_{20}^2} \theta(x_{10}^2 z - \max\{x_{21}^2, x_{20}^2\} z') \approx \frac{1}{x_{21}^2} \theta(x_{10} - x_{21}). \quad (71)$$

To simplify the second term in the curly brackets of Eq. (70) we employ the Fierz identity, which gives

$$2 \operatorname{tr} \left[V_{\underline{0}} t^a V_{\underline{1}}^{pol \dagger} t^b \right] (U_{\underline{2}})^{ba} = \operatorname{tr} \left[V_{\underline{0}} V_{\underline{2}}^\dagger \right] \operatorname{tr} \left[V_{\underline{2}} V_{\underline{1}}^{pol \dagger} \right] - \frac{1}{N_c} \operatorname{tr} \left[V_{\underline{0}} V_{\underline{1}}^{pol \dagger} \right]. \quad (72)$$

The x_2 integral in the second term of (70) is logarithmic only in the $x_{21} \ll x_{10}$ and $x_{20} \ll x_{10}$ regions. In the $x_{20} \ll x_{10}$ region Eq. (72) ensures that the expression in the double angle brackets in the second term inside the curly brackets of Eq. (70) approaches zero; thus the transverse logarithm coming from the $x_{20} \ll x_{10}$ region vanishes. This is in complete analogy with the unpolarized small- x evolution [11–18]. The physical reason behind this cancellation is that when the emitted unpolarized gluon is very close to the unpolarized quark (that it is emitted by) in the transverse plane, the system is identical to the original unpolarized quark.

In the $x_{21} \ll x_{10}$ region, however, the second term inside the curly brackets of Eq. (70) does not vanish, as again can be seen from Eq. (72). The formal reason behind this is that the zero-size polarized dipole does not have a unit S -matrix. In other words, polarized dipoles do not have the color-transparency property that the unpolarized dipoles have, since when the polarized quark line overlaps with the unpolarized anti-quark line in the transverse plane, their interactions with the target do not cancel. Somewhat more physically, one can argue that when an unpolarized gluon is emitted by a polarized quark, the system does not become equivalent to the original polarized quark even if the gluon is very close to the quark in the transverse plane.

In order to keep only the logarithmic $x_{21} \ll x_{10}$ region, we replace

$$\frac{x_{10}^2}{x_{21}^2 x_{20}^2} \rightarrow \frac{1}{x_{21}^2} \theta(x_{10} - x_{21}) \quad (73)$$

in the second term in the curly brackets of Eq. (70). With the substitutions (71) and (73), Eq. (70) becomes

$$\begin{aligned} G_{10}(zs) = G_{10}^{(0)}(zs) + \frac{\alpha_s N_c}{2\pi^2} \int_{\frac{\Lambda^2}{s}}^z \frac{dz'}{z'} \int \frac{d^2 x_2}{x_{21}^2} \theta(x_{10}^2 - x_{21}^2) \theta(x_{21}^2 - \frac{1}{z's}) \left\{ \left\langle \left\langle \frac{1}{N_c^2} \operatorname{tr} \left[V_{\underline{0}} t^a V_{\underline{1}}^\dagger t^b \right] (U_{\underline{2}}^{pol})^{ba} + \text{c.c.} \right\rangle \right\rangle (z's) \right. \\ \left. + \left\langle \left\langle \frac{1}{N_c^2} \operatorname{tr} \left[V_{\underline{0}} t^a V_{\underline{1}}^{pol \dagger} t^b \right] (U_{\underline{2}})^{ba} - \frac{C_F}{N_c^2} \operatorname{tr} \left[V_{\underline{0}} V_{\underline{1}}^{pol \dagger} \right] + \text{c.c.} \right\rangle \right\rangle (z's) \right\}. \end{aligned} \quad (74)$$

To further simplify Eq. (74), we invoke the DLA approximation (and discard all the leading-logarithmic evolution, such as BFKL, BK or JIMWLK; that is, put all the S -matrices for the dipoles without polarized Wilson lines equal to one). We also employ the large- N_c limit. With these approximations, we replace (see [9] and Appendix A of [37])

$$\left\langle \left\langle \operatorname{tr} \left[V_{\underline{0}} t^a V_{\underline{1}}^\dagger t^b \right] (U_{\underline{2}}^{pol})^{ba} \right\rangle \right\rangle \rightarrow \frac{N_c}{2} \left\langle \left\langle \operatorname{tr} \left[V_{\underline{0}} V_{\underline{2}}^{pol \dagger} \right] \right\rangle \right\rangle + \frac{N_c}{2} \left\langle \left\langle \operatorname{tr} \left[V_{\underline{2}}^{pol} V_{\underline{1}}^\dagger \right] \right\rangle \right\rangle \quad (75)$$

and obtain

$$\begin{aligned} G_{10}(zs) = G_{10}^{(0)}(zs) + \frac{\alpha_s N_c}{2\pi^2} \int_{\frac{\Lambda^2}{s}}^z \frac{dz'}{z'} \int \frac{d^2 x_2}{x_{21}^2} \theta(x_{10}^2 - x_{21}^2) \theta(x_{21}^2 - \frac{1}{z's}) \left\{ \left\langle \left\langle \frac{1}{2N_c} \operatorname{tr} \left[V_{\underline{0}} V_{\underline{2}}^{pol \dagger} \right] \right. \right. \right. \\ \left. \left. + \frac{1}{2N_c} \operatorname{tr} \left[V_{\underline{2}}^{pol} V_{\underline{1}}^\dagger \right] + \text{c.c.} \right\rangle \right\rangle (z's) + \left\langle \left\langle \frac{1}{2N_c} \operatorname{tr} \left[V_{\underline{2}} V_{\underline{1}}^{pol \dagger} \right] - \frac{1}{2N_c} \operatorname{tr} \left[V_{\underline{0}} V_{\underline{1}}^{pol \dagger} \right] + \text{c.c.} \right\rangle \right\rangle (z's) \right\}. \end{aligned} \quad (76)$$

Equation (76) has been derived for a polarized quark dipole evolution. The large- N_c limit of helicity evolution, as considered in [9, 37], involves only gluons: the corresponding dipole amplitude $G_{10}(zs)$ would correspond to the interaction of the quark line of one large- N_c gluon and the anti-quark line of another large- N_c gluon with the target [34–36]. Here lies another important difference between the small- x helicity evolution at hand and the unpolarized evolution [11–18, 34–36]: in the case of helicity evolution, the difference between a polarized gluon emission by a

polarized quark versus by a polarized gluon is not only in the color factor. For instance, for helicity splitting functions at small- z and large N_c one has $\Delta P_{GG}(z) = 4 \Delta P_{Gq}(z)$. Out of this factor of 4 difference, 2 is due to the color factors, while another 2 is due to helicity dynamics in the splitting. This means that, when going from the quark dipole of Eq. (76) to the quark part of the gluon dipole, we need to multiply the polarized gluon emission term (the first term in the curly brackets) by 2 [37]. (Ideally we would not be needing to do this “ad hoc” operation if we had started with the polarized gluon dipole operator above.) We thus have

$$G_{10}(zs) = G_{10}^{(0)}(zs) + \frac{\alpha_s N_c}{2\pi^2} \int_{\frac{\Lambda^2}{s}}^z \frac{dz'}{z'} \int \frac{d^2 x_2}{x_{21}^2} \theta(x_{10}^2 - x_{21}^2) \theta(x_{21}^2 - \frac{1}{z's}) \left\{ \left\langle \left\langle \frac{1}{N_c} \text{tr} [V_{\underline{0}} V_{\underline{2}}^{pol \dagger}] \right. \right. \right. \\ \left. \left. \left. + \frac{1}{N_c} \text{tr} [V_{\underline{2}}^{pol} V_{\underline{1}}^\dagger] + \text{c.c.} \right\rangle \right\rangle (z's) + \left\langle \left\langle \frac{1}{2N_c} \text{tr} [V_{\underline{2}} V_{\underline{1}}^{pol \dagger}] - \frac{1}{2N_c} \text{tr} [V_{\underline{0}} V_{\underline{1}}^{pol \dagger}] + \text{c.c.} \right\rangle \right\rangle (z's) \right\}. \quad (77)$$

The last step, which does not automatically follow from our formalism, is to identify whether various VV^\dagger correlators in Eq. (77) combine into the amplitude $G_{10}(zs)$ or into the auxiliary neighbor-dipole amplitude Γ . This depends on the lifetime ordering for the subsequent evolution in those dipoles. For instance, since in Eq. (77) we have $x_{21} \ll x_{10}$, the subsequent evolution in the dipole 02 in the non-eikonal emission diagrams of Fig. 2 “knows” about the dipole 21, and hence $\text{tr} [V_{\underline{0}} V_{\underline{2}}^{pol \dagger}]$ in Eq. (77) [9, 37] gives us $\Gamma_{02,21}(z's) \approx \Gamma_{01,21}(z's)$. Similarly, one can show that $\text{tr} [V_{\underline{0}} V_{\underline{1}}^{pol \dagger}]$ in Eq. (77) contributes $\Gamma_{01,21}(z's)$ [37]. The remaining traces give us G ’s. After performing this identification and integrating over impact parameters, we get

$$G(x_{10}^2, zs) = G(x_{10}^2, zs) + \frac{\alpha_s N_c}{2\pi} \int_{\frac{1}{x_{10}^2 s}}^z \frac{dz'}{z'} \int_{\frac{1}{z's}}^{\frac{x_{10}^2}{x_{21}^2}} \frac{dx_{21}^2}{x_{21}^2} [\Gamma(x_{10}^2, x_{21}^2, z's) + 3G(x_{21}^2, z's)], \quad (78)$$

in agreement with Eq. (12a). (To arrive at Eq. (78) one also needs to notice that, due to the bounds of the x_{21} integral, $z' > 1/(x_{21}^2 s) > 1/(x_{10}^2 s)$ which is a stronger lower bound on the z' integration than Λ^2/s of Eq. (77).) Eq. (12b) is obtained by analogy, with a slightly more subtle way of imposing the lifetime ordering.

B. Evolution of the Polarized Dipole Operator For the Dipole Gluon Helicity

The dipole gluon helicity distribution is governed by the polarized dipole amplitude (37) and the (local) polarized Wilson line (34). Written explicitly, this operator is

$$G_{10}^i(zs) = \frac{p^+}{2N_c} \int_{-\infty}^{\infty} dx_1^- \langle \text{tr} [V_{\underline{0}} V_{\underline{1}}[-\infty, x_1^-] (-ig) A_{\perp}^i(x_1^-, \underline{x}_1) V_{\underline{1}}[x_1^-, \infty]] + \text{c.c.} \rangle (zs). \quad (79)$$

In the same way as before, we expand the fields in terms of classical and quantum components, contracting the lowest-order contributions in the quantum fields. Again, there are three general classes of contractions / diagrams: “polarized ladder” emissions (IV and IV’), “polarized non-ladder” emissions (V and V’), and unpolarized emissions

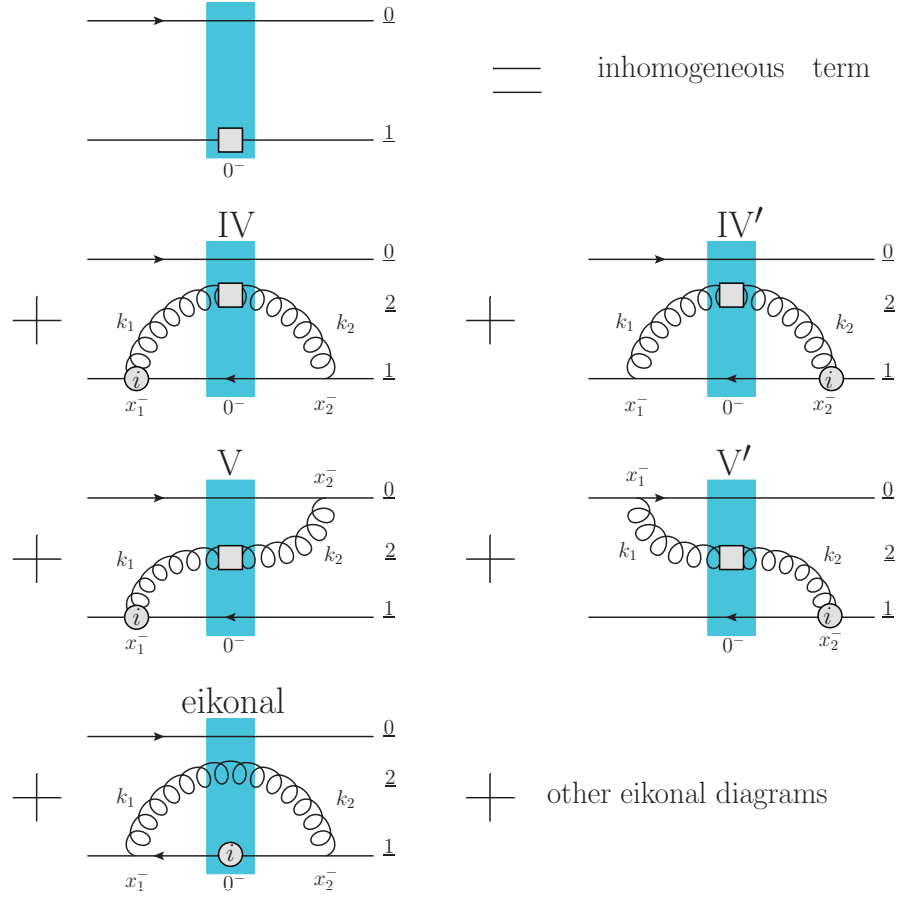


FIG. 3. Diagrams illustrating contractions contributing the evolution of the polarized dipole amplitude for the dipole gluon helicity distribution. The blue band represents the classical gluon fields (shock wave), the vertex (i) denotes the sub-eikonal operator insertion, and the gray box represents the polarized Wilson line.

(“eikonal”), as illustrated in Fig. 3. In analogy to Eq. (57), the specific contractions are

$$\text{IV :} \quad \text{tr} \left[V_{\underline{0}} \overbrace{V_{\underline{1}}[-\infty, x_1^-] a_{\perp}^i(x_1^-, \underline{x}_1)} V_{\underline{1}}[x_1^-, \infty] \right] \quad (80a)$$

$$\text{IV' :} \quad \text{tr} \left[V_{\underline{0}} \overbrace{V_{\underline{1}}[-\infty, x_1^-] a_{\perp}^i(x_1^-, \underline{x}_1)} V_{\underline{1}}[x_1^-, \infty] \right] \quad (80b)$$

$$\text{V + V' :} \quad \text{tr} \left[V_{\underline{0}} \overbrace{V_{\underline{1}}[-\infty, x_1^-] a_{\perp}^i(x_1^-, \underline{x}_1)} V_{\underline{1}}[x_1^-, \infty] \right] \quad (80c)$$

$$\begin{aligned} \text{eikonal :} \quad & \text{tr} \left[V_{\underline{0}} \overbrace{V_{\underline{1}}[-\infty, x_1^-] A_{cl\perp}^i(x_1^-, \underline{x}_1)} V_{\underline{1}}[x_1^-, \infty] \right] \\ & + \text{tr} \left[V_{\underline{0}} \overbrace{V_{\underline{1}}[-\infty, x_1^-] A_{cl\perp}^i(x_1^-, \underline{x}_1)} V_{\underline{1}}[x_1^-, \infty] \right] \\ & + \text{tr} \left[V_{\underline{0}} \overbrace{V_{\underline{1}}[-\infty, x_1^-] A_{cl\perp}^i(x_1^-, \underline{x}_1)} V_{\underline{1}}[x_1^-, \infty] \right] \\ & + \text{tr} \left[V_{\underline{0}} \overbrace{V_{\underline{1}}[-\infty, x_1^-] A_{cl\perp}^i(x_1^-, \underline{x}_1)} V_{\underline{1}}[x_1^-, \infty] \right] \\ & + \text{tr} \left[V_{\underline{0}} \overbrace{V_{\underline{1}}[-\infty, x_1^-] A_{cl\perp}^i(x_1^-, \underline{x}_1)} V_{\underline{1}}[x_1^-, \infty] \right] \\ & + \text{tr} \left[V_{\underline{0}} \overbrace{V_{\underline{1}}[-\infty, x_1^-] A_{cl\perp}^i(x_1^-, \underline{x}_1)} V_{\underline{1}}[x_1^-, \infty] \right] \\ & + \text{tr} \left[V_{\underline{0}} \overbrace{V_{\underline{1}}[-\infty, x_1^-] A_{cl\perp}^i(x_1^-, \underline{x}_1)} V_{\underline{1}}[x_1^-, \infty] \right]. \end{aligned} \quad (80d)$$

As we saw in Eqs. (65) and (67), the propagator for the ladder diagram I or IV is just a special case of the propagator for the non-ladder diagram II or V. We therefore begin by calculating diagram V, which is the contraction of the operator insertion with the unpolarized Wilson line in the time ordering $x_1^- < 0 < x_2^-$. Expanding the unpolarized Wilson line gives

$$\begin{aligned} (\delta G_{10}^i)_V(zs) &= \frac{g^2 p^+}{2N_c} \int_{-\infty}^0 dx_1^- \int_0^\infty dx_2^- \left\langle \text{tr} \left[V_{\underline{0}} \overbrace{a_{\perp}^i(x_1^-, \underline{x}_1)} V_{\underline{1}}^\dagger a^+(x_2^-, x_0) \right] + \text{c.c.} \right\rangle \\ &= \frac{g^2 p^+}{2N_c} \left\langle \text{tr} \left[V_{\underline{0}} t^a V_{\underline{1}}^\dagger t^b \right] (\Delta_{cl}^{i+})_{pol}^{ba}(\underline{x}_1, \underline{x}_0) + \text{c.c.} \right\rangle, \end{aligned} \quad (81)$$

where we have defined the propagator in the classical background field as

$$(\Delta_{cl}^{i+})_{pol}^{ba}(\underline{x}_1, \underline{x}_0) \equiv \int_{-\infty}^0 dx_1^- \int_0^\infty dx_2^- \overbrace{a_{\perp}^{ia}(x_1^-, \underline{x}_1)} a^{+b}(x_2^-, x_0). \quad (82)$$

As before, we will find that the propagator $\Delta_{cl}^{\mu\nu}$ is symmetric, such that all of the polarized emissions shown in Fig. 3 can be written as

$$(\delta G_{10}^i)_{IV}(zs) = (\delta G_{10}^i)_{IV'}(zs) = -\frac{g^2 p^+}{2N_c} \left\langle \text{tr} \left[V_{\underline{0}} t^a V_{\underline{1}}^\dagger t^b \right] (\Delta_{cl}^{i+})_{pol}^{ba}(\underline{x}_1, \underline{x}_1) + \text{c.c.} \right\rangle \quad (83a)$$

$$(\delta G_{10}^i)_V(zs) = (\delta G_{10}^i)_{V'}(zs) = \frac{g^2 p^+}{2N_c} \left\langle \text{tr} \left[V_{\underline{0}} t^a V_{\underline{1}}^\dagger t^b \right] (\Delta_{cl}^{i+})_{pol}^{ba}(\underline{x}_1, \underline{x}_0) + \text{c.c.} \right\rangle. \quad (83b)$$

The two classes of diagrams differ only in two respects: a sign difference in the prefactor (due to expanding $V_{\underline{0}}$ vs. $V_{\underline{1}}^\dagger$) and the arguments of the propagator (for ladder vs. non-ladder emissions).

Thus the calculation is reduced to finding the propagator (82). In analogy to Eq. (62), we write the propagator as

$$\begin{aligned}
(\Delta_{cl}^{i+})_{pol}^{ba}(\underline{x}_1, \underline{x}_0) &= \sum_{\lambda} \lambda \int d^2 x_2 \left[\int_{-\infty}^0 dx_1^- \int \frac{d^4 k_1}{(2\pi)^4} e^{ik_1^+ x_1^-} e^{ik_1 \cdot \underline{x}_{21}} \frac{-i}{k_1^2 + i\epsilon} (\epsilon_{\lambda}^*)^i_{\perp} \right] \\
&\quad \times \left[(U_{\underline{2}}^{pol})^{ba} (2k_1^-) 2\pi \delta(k_1^- - k_2^-) \right] \\
&\quad \times \left[\int_0^{\infty} dx_2^- \int \frac{d^4 k_2}{(2\pi)^4} e^{-ik_2^+ x_2^-} e^{-ik_2 \cdot \underline{x}_{20}} \frac{-i}{k_2^2 + i\epsilon} [\epsilon_{\lambda}(k_2)]^+ \right] \\
&= -\frac{i}{\pi} \epsilon_T^{ij} \int dk^- \int d^2 x_2 \left[\int_{-\infty}^0 dx_1^- \int \frac{d^2 k_1 dk_1^+}{(2\pi)^3} e^{ik_1^+ x_1^-} e^{ik_1 \cdot \underline{x}_{21}} \frac{1}{k_1^2 + i\epsilon} \right] \\
&\quad \times \left[\int_0^{\infty} dx_2^- \int \frac{d^2 k_2 dk_2^+}{(2\pi)^3} e^{-ik_2^+ x_2^-} e^{-ik_2 \cdot \underline{x}_{20}} \frac{1}{k_2^2 + i\epsilon} (k_2)^j_{\perp} \right] (U_{\underline{2}}^{pol})^{ba}. \tag{84}
\end{aligned}$$

Employing the integrals in (64) we recast this as

$$(\Delta_{cl}^{i+})_{pol}^{ba}(\underline{x}_1, \underline{x}_0) = -\frac{1}{4\pi^3} \int dk^- \int d^2 x_2 \ln \frac{1}{x_{21}\Lambda} \frac{\epsilon_T^{ij}(x_{20})^j_{\perp}}{x_{20}^2} (U_{\underline{2}}^{pol})_{(k^-)}^{ba}. \tag{85}$$

With the propagator (85), it is straightforward to obtain the evolution kernels IV – V':

$$\begin{aligned}
(\delta G_{10}^i)_{IV}(zs) &= (\delta G_{10}^i)_{IV'}(zs) \\
&= \frac{\alpha_s N_c}{4\pi^2} \int_{\frac{\Lambda^2}{s}}^z \frac{dz'}{z'} \int d^2 x_2 \ln \frac{1}{x_{21}\Lambda} \frac{\epsilon_T^{ij}(x_{21})^j_{\perp}}{x_{21}^2} \left\langle \frac{1}{N_c^2} \text{tr} [V_0 t^a V_1^{\dagger} t^b] (U_{\underline{2}}^{pol})^{ba} + \text{c.c.} \right\rangle (z's), \tag{86a}
\end{aligned}$$

$$\begin{aligned}
(\delta G_{10}^i)_V(zs) &= (\delta G_{10}^i)_{V'}(zs) \\
&= -\frac{\alpha_s N_c}{4\pi^2} \int_{\frac{\Lambda^2}{s}}^z \frac{dz'}{z'} \int d^2 x_2 \ln \frac{1}{x_{21}\Lambda} \frac{\epsilon_T^{ij}(x_{20})^j_{\perp}}{x_{20}^2} \left\langle \frac{1}{N_c^2} \text{tr} [V_0 t^a V_1^{\dagger} t^b] (U_{\underline{2}}^{pol})^{ba} + \text{c.c.} \right\rangle (z's). \tag{86b}
\end{aligned}$$

The only other ingredient necessary is the unpolarized eikonal gluon contribution, which is identical to (69) except for the replacement of the polarized Wilson lines $V_{\underline{1}}^{pol \dagger} \rightarrow (V_{\underline{1}}^{pol \dagger})^i_{\perp}$:

$$\begin{aligned}
(\delta G_{10}^i)_{\text{eik}}(zs) &= \frac{\alpha_s N_c}{2\pi^2} \int_{\frac{\Lambda^2}{s}}^z \frac{dz'}{z'} \int d^2 x_2 \frac{x_{10}^2}{x_{21}^2 x_{20}^2} \left\langle \frac{1}{N_c^2} \text{tr} [V_0 t^a (V_{\underline{1}}^{pol \dagger})^i_{\perp} t^b] (U_{\underline{2}})^{ba} \right. \\
&\quad \left. - \frac{C_F}{N_c^2} \text{tr} [V_0 (V_{\underline{1}}^{pol \dagger})^i_{\perp}] + \text{c.c.} \right\rangle (z's). \tag{87}
\end{aligned}$$

Including all these contributions, we can immediately write down the evolution equation for the polarized dipole

amplitude G_{10}^i as

$$\begin{aligned}
G_{10}^i(zs) &= G_{10}^{i(0)}(zs) + 2(\delta G_{10}^i)_{\text{IV}}(zs) + 2(\delta G_{10}^i)_{\text{V}}(zs) + (\delta G_{10}^i)_{\text{eik}}(zs) \\
&= G_{10}^{i(0)}(zs) + \frac{\alpha_s N_c}{2\pi^2} \int_{\frac{\Lambda^2}{s}}^z \frac{dz'}{z'} \int d^2x_2 \\
&\quad \times \left\{ \ln \frac{1}{x_{21}\Lambda} \epsilon_T^{ij} \left[\frac{(x_{21})_{\perp}^j}{x_{21}^2} - \frac{(x_{20})_{\perp}^j}{x_{20}^2} \right] \left\langle \left\langle \frac{1}{N_c} \text{tr} [V_0 t^a V_1^\dagger t^b] (U_2^{pol})^{ba} + \text{c.c.} \right\rangle \right\rangle (z's) \right. \\
&\quad \left. + \frac{x_{10}^2}{x_{21}^2 x_{20}^2} \left\langle \left\langle \frac{1}{N_c} \text{tr} [V_0 t^a (V_1^{pol\dagger})_{\perp}^i t^b] (U_2)^{ba} - \frac{C_F}{N_c} \text{tr} [V_0 (V_1^{pol\dagger})_{\perp}^i] + \text{c.c.} \right\rangle \right\rangle (z's) \right\}. \quad (88)
\end{aligned}$$

As expected, this evolution equation represents just the first of an infinite tower of operator equations; we will remedy this problem in the usual way by taking the large- N_c limit. We will also linearize the evolution equation, keeping the essential polarization-dependent dipoles and neglecting additional unpolarized rescattering (e.g., the non-linear saturation corrections); this will be necessary to generate double logarithms of energy. With these simplifications, we replace⁵

$$\begin{aligned}
\frac{1}{N_c^2} \text{tr} [V_0 t^a V_1^\dagger t^b] (U_2^{pol})^{ba} + \text{c.c.} &\rightarrow \\
&\rightarrow \frac{1}{N_c} \text{tr} [V_0 V_2^{pol\dagger}] + \frac{1}{N_c} \text{tr} [V_2^{pol} V_1^\dagger] + \text{c.c.} \quad (89a)
\end{aligned}$$

$$\begin{aligned}
\frac{1}{N_c^2} \text{tr} [V_0 t^a (V_1^{pol\dagger})_{\perp}^i t^b] (U_2)^{ba} - \frac{C_F}{N_c^2} \text{tr} [V_0 (V_1^{pol\dagger})_{\perp}^i] + \text{c.c.} &\rightarrow \\
&\rightarrow \frac{1}{2N_c} \text{tr} [V_2 (V_1^{pol\dagger})_{\perp}^i] - \frac{1}{2N_c} \text{tr} [V_0 (V_1^{pol\dagger})_{\perp}^i] + \text{c.c.}, \quad (89b)
\end{aligned}$$

giving

$$\begin{aligned}
G_{10}^i(zs) &= G_{10}^{i(0)}(zs) + \frac{\alpha_s N_c}{2\pi^2} \int_{\frac{\Lambda^2}{s}}^z \frac{dz'}{z'} \int d^2x_2 \\
&\quad \times \left\{ \ln \frac{1}{x_{21}\Lambda^2} \epsilon_T^{ij} \left[\frac{(x_{21})_{\perp}^j}{x_{21}^2} - \frac{(x_{20})_{\perp}^j}{x_{20}^2} \right] \left\langle \left\langle \frac{1}{2N_c} \text{tr} [V_0 V_2^{pol\dagger}] + \frac{1}{2N_c} \text{tr} [V_2^{pol} V_1^\dagger] + \text{c.c.} \right\rangle \right\rangle (z's) \right. \\
&\quad \left. + \frac{x_{10}^2}{x_{21}^2 x_{20}^2} \left\langle \left\langle \frac{1}{2N_c} \text{tr} [V_2 (V_1^{pol\dagger})_{\perp}^i] - \frac{1}{2N_c} \text{tr} [V_0 (V_1^{pol\dagger})_{\perp}^i] + \text{c.c.} \right\rangle \right\rangle (z's) \right\}. \quad (90)
\end{aligned}$$

The right-hand side of Eq. (90) are now polarized dipole amplitudes, but we must think carefully before identifying them with G or G^i . Depending on the precise limits of the x_2 integration, these dipoles may instead be “neighbor dipoles” Γ or Γ^i . These limits, in turn, are dictated by the regions of transverse phase space which generate the greatest logarithmic enhancement of the evolution.

Consider first the unpolarized eikonal emissions in the last line of Eq. (90). Just like in the quark helicity case, we see that the dipole BFKL kernel $x_{10}^2/(x_{21}^2 x_{20}^2)$ is potentially DLA in both the $x_{21}^2 \ll x_{10}^2$ limit and in the $x_{20}^2 \ll x_{10}^2$ limit. In the latter case, $\underline{x}_2 \rightarrow \underline{x}_0$, however, the operators multiplying the kernel cancel and destroy the DLA contribution. Therefore, similar to the quark case [9], we conclude that only the $x_{21}^2 \ll x_{10}^2$ region in that term is DLA and simplify the dipole BFKL kernel to $\frac{1}{x_{21}^2} \theta(x_{10}^2 - x_{21}^2) \theta(x_{21}^2 - \frac{1}{z's})$, where the available energy $z's$ acts as a UV cutoff. For each of the associated dipoles $\text{tr} [V_2 (V_1^{pol\dagger})_{\perp}^i]$ and $\text{tr} [V_0 (V_1^{pol\dagger})_{\perp}^i]$, we must impose a lifetime ordering condition on their subsequent evolution to ensure that the “fast” quantum fields computed here live longer than the “slow” classical fields. The first term $\text{tr} [V_2 (V_1^{pol\dagger})_{\perp}^i]$ depends only on the distance x_{21} associated with the quantum fluctuation and

⁵ Note that Eq. (75) suggested in Appendix A of [37] is missing an overall factor of 2 on its right-hand side [59]. The correct version of equation (75) would lead directly to Eq. (77), bypassing Eq. (76) above and the discussion that follows [59]. This factor of 2 is included in obtaining Eqs. (89).

can be identified as $G_{12}^i(z's)$. The second term $\text{tr} [V_0(V_1^{\text{pol}\dagger})^i]$ appears to depend only on the distance x_{10} , but must also respect the lifetime ordering with respect to the virtual gluon loop of transverse size x_{21} that gave rise to this term in the equation. This term is therefore a neighbor dipole $\Gamma_{10,21}^i(z's)$ because it “remembers” about the lifetime of the neighboring x_{21} quantum fluctuation (see [37] for a detailed calculation explaining this conclusion). We therefore simplify the eikonal terms to write

$$\begin{aligned}
G_{10}^i(zs) = & G_{10}^{i(0)}(zs) + \frac{\alpha_s N_c}{2\pi^2} \int_{\frac{\Lambda^2}{s}}^z \frac{dz'}{z'} \int d^2x_2 \\
& \times \left\{ \ln \frac{1}{x_{21}^2 \Lambda^2} \epsilon_T^{ij} \left[\frac{(x_{21})_{\perp}^j}{x_{21}^2} - \frac{(x_{20})_{\perp}^j}{x_{20}^2} \right] \left\langle \left\langle \frac{1}{2N_c} \text{tr} [V_0 V_2^{\text{pol}\dagger}] + \frac{1}{2N_c} \text{tr} [V_2^{\text{pol}} V_1^\dagger] + \text{c.c.} \right\rangle \right\rangle (z's) \right\} \\
& + \frac{\alpha_s N_c}{2\pi^2} \int_{\frac{\Lambda^2}{s}}^z \frac{dz'}{z'} \int \frac{d^2x_2}{x_{21}^2} \theta(x_{10}^2 - x_{21}^2) \theta(x_{21}^2 - \frac{1}{z's}) [G_{12}^i(z's) - \Gamma_{10,21}^i(z's)]. \quad (91)
\end{aligned}$$

The story for the polarized gluon emissions in the second line of Eq. (91), however, is significantly more complicated. The reason is that the transverse integration does not generate a logarithm of the energy, so the whole kernel is not DLA. (After integration, $\ln \frac{1}{x_{21} \Lambda}$ becomes $\ln \frac{1}{x_{10} \Lambda}$ and not a logarithm of the energy.) It would seem, then, that the polarized emissions only generate one logarithm of energy from the z' integral and can be neglected compared to the DLA evolution of the eikonal terms.

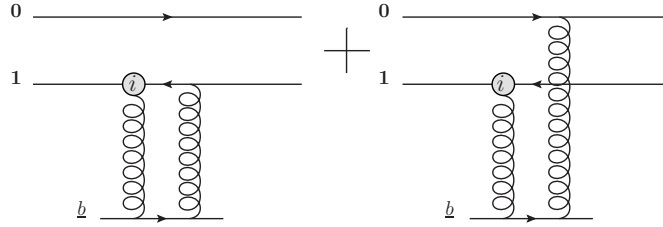


FIG. 4. Diagrams contributing the initial conditions for G^i and Γ^i in Eq. (93).

This, however, is not quite the case, because of the initial conditions. The initial conditions for the polarized dipole operator G_{10}^i , taken in the quark target model at a fixed impact parameter, can be obtained by computing the diagrams shown in Fig. 4:

$$G_{10}^{i(0)}(z) = \Gamma_{10,21}^{i(0)}(z) = -\frac{\alpha_s^2 C_F}{N_c} \epsilon^{ij} \frac{(x_1 - b)^j}{|x_1 - b|^2} \ln \frac{|x_1 - b|}{|x_0 - b|}. \quad (92)$$

Integrating over the impact parameters yields

$$\int d^2b_{10} G_{10}^{i(0)}(zs) = \int d^2b_{10} \Gamma_{10,21}^{i(0)}(zs) = -\frac{\alpha_s^2 C_F}{N_c} \pi \epsilon^{ij} x_{10}^j \ln \frac{1}{x_{10} \Lambda}, \quad (93)$$

which is independent of the energy. By contrast, the dipoles $\text{tr} [V_0 V_2^{\text{pol}\dagger}]$ and $\text{tr} [V_2^{\text{pol}} V_1^\dagger]$ in Eq. (91) are the ones which enter the evolution (12) of the quark helicity distribution. Their initial conditions are given by Eq. (13b) in [37] for the impact-parameter integrated case. Keeping only the gluon-exchange part of that expression,

$$\int d^2b_{10} G_{10}^{(0)}(zs) = \int d^2b_{10} \Gamma_{10,21}^{(0)}(zs) = -\frac{\alpha_s^2 C_F}{N_c} \pi \ln(zs x_{10}^2), \quad (94)$$

we see that $\int d^2b_{10} G_{10}^i$ in (93) is suppressed by a logarithm of energy compared to $\int d^2b_{10} G_{10}$ in (94).

This implies that G^i starts energy-independent and, after one step of eikonal evolution, acquires two logarithms of energy. On the other hand, G and Γ can mix into G^i through the second line of Eq. (91), picking up one logarithm of energy from the evolution. But since G and Γ start off with one logarithm of energy from the initial conditions, both of these two contributions are of the same order. Subsequent evolution in the eikonal $G^i, \Gamma^i \rightarrow G^i, \Gamma^i$ channel and the prior evolution (12) in the polarized $G, \Gamma \rightarrow G, \Gamma$ channel, are both double logarithmic.

Therefore, we conclude that we must keep all of Eq. (91), and we are left with a transverse integral for the polarized emissions which covers the entire plane. The resulting kernel in the second line of Eq. (91) is leading-logarithmic (LLA). This is similar to the unpolarized BFKL/BK/JIMWLK evolution, which also has a LLA kernel, without any logarithm of energy coming from the transverse coordinate integral. In the unpolarized evolution case at LLA one does not need to impose the lifetime ordering condition which would restrict the transverse integrals (see [45, 60] for the higher-order corrections though). The same is true here: the transverse integral in the second line of Eq. (91) is unconstrained.

This leads to a problem though: with an unconstrained integral the second line of Eq. (91) we cannot tell whether the dipole 21 is smaller than the dipole 20 ($x_{21} \ll x_{20}$) or vice versa ($x_{20} \ll x_{21}$) or both dipoles are large $x_{21} \sim x_{20} \gg x_{10}$. This was not necessary for the LLA unpolarized dipole evolution [34, 35, 61], since there the subsequent evolution in all the daughter dipoles was independent of other dipoles and their sizes. This is not the case for our DLA helicity evolution (12), where the subsequent evolution in a given dipole can make it a “neighbor dipole” if the adjacent dipole (produced in the same step of evolution) was smaller in the transverse plane.

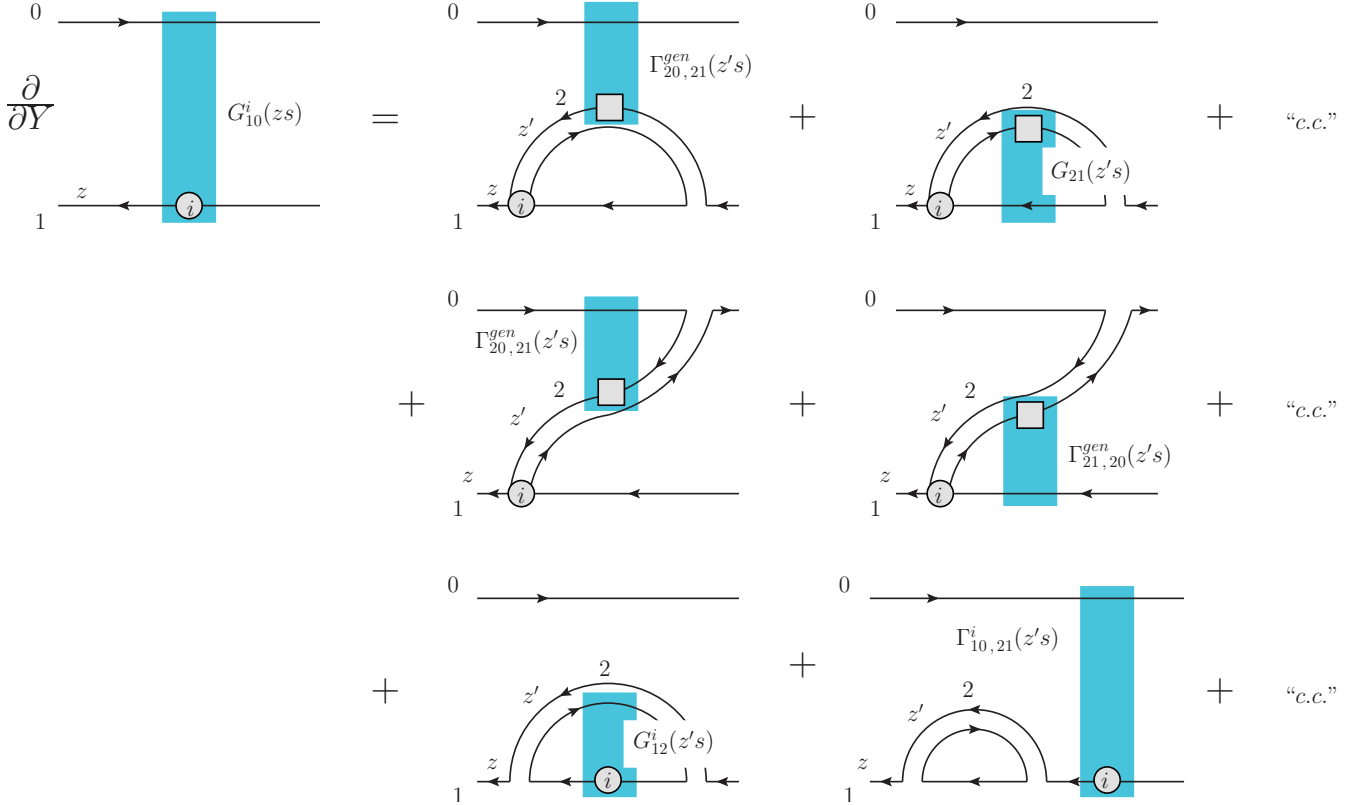


FIG. 5. Linearized large- N_c evolution of the new dipole function G^i as written in Eq. (96a). Because there is no universal DLA parameter for the various terms, we have no a priori constraint on the relative sizes of x_{20} and x_{21} , which makes enforcing lifetime ordering in these dipoles more subtle. We must distinguish between the ladder emission of polarized gluons (top line), which are constrained by the lifetime of dipole 21 only, and the non-ladder emission of polarized gluons (middle line), which are constrained by the lifetimes of both dipoles 20 and 21. The “+ c.c.” stands for adding mirror-reflected diagrams as well as the true complex conjugates in which line 0 becomes a polarized quark line.

By our power counting, the subsequent evolution for the correlators in the second line of Eq. (91) should be DLA. Hence it should be expressed in terms of the DLA amplitudes G and Γ . Consider specifically diagram V in Fig. 3. When $x_{20} \ll x_{21}$, the subsequent evolution in dipole 20 is given by $G_{20}(z's)$. Conversely, when $x_{21} \ll x_{20}$, the subsequent evolution in dipole 20 is given by $\Gamma_{20,21}(z's)$. With the DLA accuracy of this subsequent evolution we can not distinguish, say, $x_{21} < x_{20}$ from $x_{21} \ll x_{20}$. Therefore, to include both the $x_{21} < x_{20}$ and $x_{21} > x_{20}$ regions of integration in the second line of Eq. (91) we define a new amplitude

$$\Gamma_{20,21}^{gen}(z's) = \theta(x_{20} - x_{21}) \Gamma_{20,21}(z's) + \theta(x_{21} - x_{20}) G_{20}(z's). \quad (95)$$

This amplitude Γ^{gen} encompasses both regions of transverse plane with the DLA accuracy, and is thus the proper

amplitude to use for diagrams IV, IV' in Fig. 3 when describing the subsequent evolution in dipole 20 and in diagrams V, V' when describing the evolution in either of the daughter dipoles, 20 or 21.

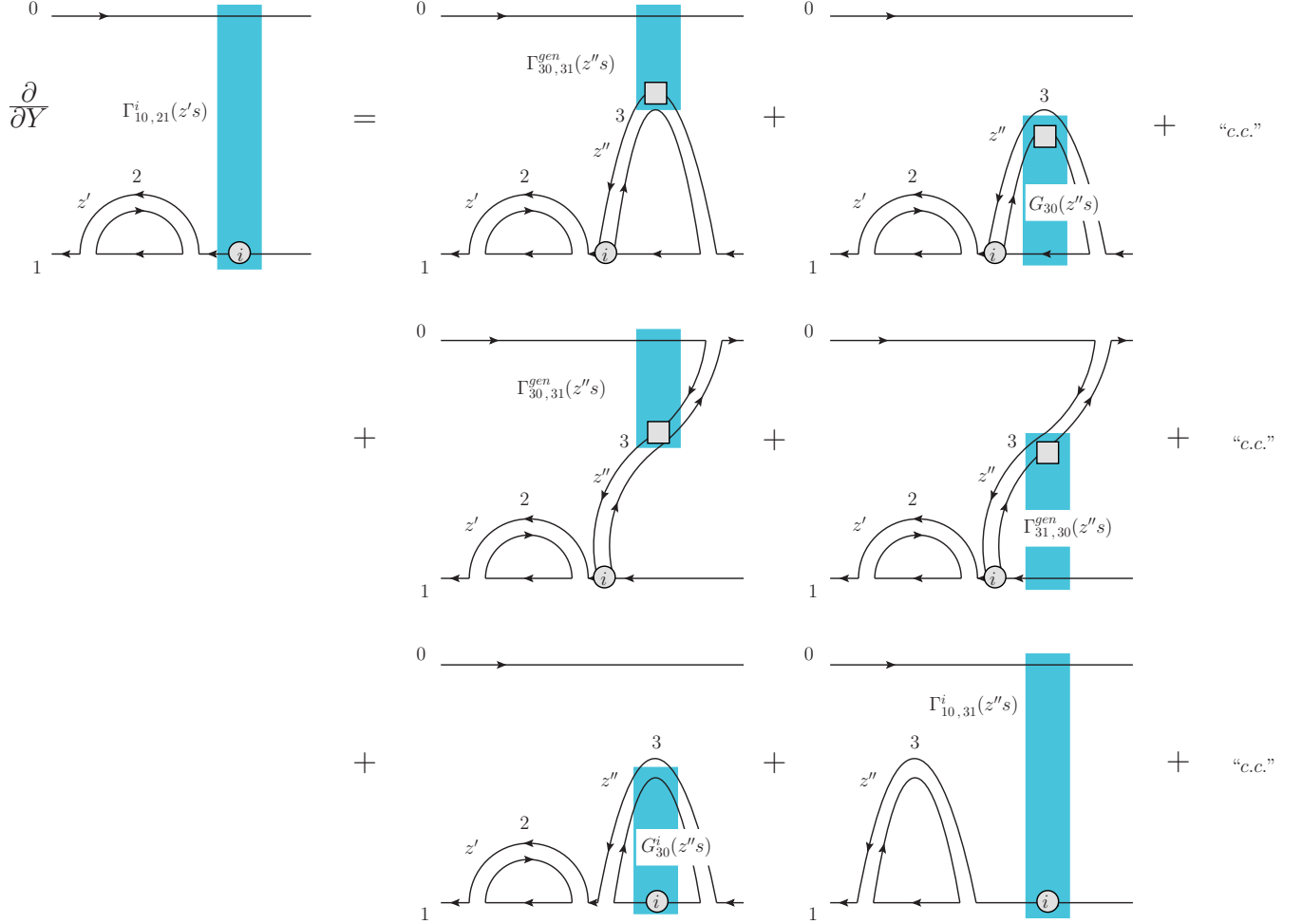


FIG. 6. Linearized large- N_c evolution of the new dipole function Γ^i as written in Eq. (96b). Because there is no universal DLA parameter for the various terms, we have no a priori constraint on the relative sizes of x_{30} and x_{31} , which makes enforcing lifetime ordering in these dipoles more subtle. We must distinguish between the ladder emission of polarized gluons (top line), which are constrained by the lifetime of dipole 31 only, and the non-ladder emission of polarized gluons (middle line), which are constrained by the lifetimes of both dipoles 30 and 31. The “+ c.c.” stands for adding mirror-reflected diagrams as well as the true complex conjugates in which line 1 becomes a polarized quark line.

As a result of this analysis, we obtain the large- N_c evolution equations relevant for the dipole gluon helicity

distribution,

$$\begin{aligned}
G_{10}^i(zs) &= G_{10}^{i(0)}(zs) + \frac{\alpha_s N_c}{2\pi^2} \int_{\frac{\Lambda^2}{s}}^z \frac{dz'}{z'} \int d^2x_2 \ln \frac{1}{x_{21}^2 \Lambda^2} \frac{\epsilon_T^{ij}(x_{21})_{\perp}^j}{x_{21}^2} \left[\Gamma_{20,21}^{gen}(z's) + G_{21}(z's) \right] \\
&\quad - \frac{\alpha_s N_c}{2\pi^2} \int_{\frac{\Lambda^2}{s}}^z \frac{dz'}{z'} \int d^2x_2 \ln \frac{1}{x_{21}^2 \Lambda^2} \frac{\epsilon_T^{ij}(x_{20})_{\perp}^j}{x_{20}^2} \left[\Gamma_{20,21}^{gen}(z's) + \Gamma_{21,20}^{gen}(z's) \right] \\
&\quad + \frac{\alpha_s N_c}{2\pi^2} \int_{\frac{1}{x_{10}^2 s}}^z \frac{dz'}{z'} \int \frac{d^2x_2}{x_{21}^2} \theta(x_{10}^2 - x_{21}^2) \theta(x_{21}^2 - \frac{1}{z's}) \left[G_{12}^i(z's) - \Gamma_{10,21}^i(z's) \right], \tag{96a}
\end{aligned}$$

$$\begin{aligned}
\Gamma_{10,21}^i(z's) &= G_{10}^{i(0)}(z's) + \frac{\alpha_s N_c}{2\pi^2} \int_{\frac{\Lambda^2}{s}}^{z'} \frac{dz''}{z''} \int d^2x_3 \ln \frac{1}{x_{31}^2 \Lambda^2} \frac{\epsilon_T^{ij}(x_{31})_{\perp}^j}{x_{31}^2} \left[\Gamma_{30,31}^{gen}(z''s) + G_{31}(z''s) \right] \\
&\quad - \frac{\alpha_s N_c}{2\pi^2} \int_{\frac{\Lambda^2}{s}}^{z'} \frac{dz''}{z''} \int d^2x_3 \ln \frac{1}{x_{31}^2 \Lambda^2} \frac{\epsilon_T^{ij}(x_{30})_{\perp}^j}{x_{30}^2} \left[\Gamma_{30,31}^{gen}(z''s) + \Gamma_{31,30}^{gen}(z''s) \right] \\
&\quad + \frac{\alpha_s N_c}{2\pi^2} \int_{\frac{1}{x_{10}^2 s}}^{z'} \frac{dz''}{z''} \int \frac{d^2x_3}{x_{31}^2} \theta\left(\min\left[x_{10}^2, x_{21}^2 \frac{z'}{z''}\right] - x_{31}^2\right) \theta\left(x_{31}^2 - \frac{1}{z''s}\right) \left[G_{13}^i(z''s) - \Gamma_{10,31}^i(z''s) \right], \tag{96b}
\end{aligned}$$

which are illustrated in Figs. 5 and 6. The solution of these equations with the help of Eq. (40) will give us the small- x asymptotics of the dipole gluon helicity TMD and, through this, of the gluon helicity PDF.

V. SOLUTION OF THE EVOLUTION EQUATIONS FOR THE DIPOLE GLUON HELICITY

A. Structure of the Evolution Equations

We will now proceed to simplify and solve the evolution equations (96) for the polarized dipole amplitude G_{10}^i at small x . First, it is convenient to convert from the vector quantity $G_{10}^i(zs)$ to the scalar functions $G_1(x_{10}^2, zs)$ and $G_2(x_{10}^2, zs)$ by integrating over impact parameters $\int d^2b_{10} = \int d^2b_{20} = \int d^2b_{21}$ and using the decomposition (39). The same decomposition is applied to the impact-parameter integral of $\Gamma_{10,21}^i(z's)$. From Eq. (41), we see that the dipole gluon helicity distribution couples to the G_2 function, which can be extracted using the projection

$$G_2(x_{10}^2, zs) = -\frac{(x_{10})_{\perp}^i \epsilon_T^{ij}}{x_{10}^2} \int d^2b_{10} G_{10}^j(zs). \tag{97}$$

In doing the impact parameter integral, the G_{12}^i term from the unpolarized eikonal evolution (third line of (96a)) drops out due to the angular integration. Similarly, the G_{21} term in the polarized ladder evolution (first line of (96a)) appears to vanish due to the angular integral. However, the radial integral in the kernel is potentially IR divergent without this term, so we will keep this contribution for now. After performing the impact parameter integral of

Eqs. (96) along with the projection (97), we obtain

$$\begin{aligned}
G_2(x_{10}^2, zs) &= G_2^{(0)}(x_{10}^2, zs) + \frac{\alpha_s N_c}{2\pi^2} \int_{\frac{\Lambda^2}{s}}^z \frac{dz'}{z'} \int d^2x_2 \ln \frac{1}{x_{21}^2 \Lambda^2} \frac{x_{10} \cdot x_{21}}{x_{10}^2 x_{21}^2} \left[\Gamma_{gen}(x_{20}^2, x_{21}^2, z's) + G(x_{21}^2, z's) \right] \\
&\quad - \frac{\alpha_s N_c}{2\pi^2} \int_{\frac{\Lambda^2}{s}}^z \frac{dz'}{z'} \int d^2x_2 \ln \frac{1}{x_{21}^2 \Lambda^2} \frac{x_{10} \cdot x_{20}}{x_{10}^2 x_{20}^2} \left[\Gamma_{gen}(x_{20}^2, x_{21}^2, z's) + \Gamma_{gen}(x_{21}^2, x_{20}^2, z's) \right] \\
&\quad - \frac{\alpha_s N_c}{2\pi} \int_{\frac{1}{x_{10}^2 s}}^z \frac{dz'}{z'} \int_{\frac{1}{z's}}^{x_{10}^2} \frac{dx_{21}^2}{x_{21}^2} \Gamma_2(x_{10}^2, x_{21}^2, z's), \tag{98a}
\end{aligned}$$

$$\begin{aligned}
\Gamma_2(x_{10}^2, x_{21}^2, z's) &= G_2^{(0)}(x_{10}^2, z's) + \frac{\alpha_s N_c}{2\pi^2} \int_{\frac{\Lambda^2}{s}}^{z'} \frac{dz''}{z''} \int d^2x_3 \ln \frac{1}{x_{31}^2 \Lambda^2} \frac{x_{10} \cdot x_{31}}{x_{10}^2 x_{31}^2} \left[\Gamma_{gen}(x_{30}^2, x_{31}^2, z''s) + G(x_{31}^2, z's) \right] \\
&\quad - \frac{\alpha_s N_c}{2\pi^2} \int_{\frac{\Lambda^2}{s}}^{z'} \frac{dz''}{z''} \int d^2x_3 \ln \frac{1}{x_{31}^2 \Lambda^2} \frac{x_{10} \cdot x_{30}}{x_{10}^2 x_{30}^2} \left[\Gamma_{gen}(x_{30}^2, x_{31}^2, z''s) + \Gamma_{gen}(x_{31}^2, x_{30}^2, z''s) \right] \\
&\quad - \frac{\alpha_s N_c}{2\pi} \int_{\frac{1}{x_{10}^2 s}}^{z'} \frac{dz''}{z''} \int_{\frac{1}{z''s}}^{\min[x_{10}^2, x_{21}^2 \frac{z'}{z''}]} \frac{dx_{31}^2}{x_{31}^2} \Gamma_2(x_{10}^2, x_{31}^2, z''s). \tag{98b}
\end{aligned}$$

We have defined an impact-parameter integrated amplitude Γ_{gen} by (cf. Eq. (95))

$$\Gamma_{gen}(x_{20}, x_{21}, z's) = \theta(x_{20} - x_{21}) \Gamma(x_{20}, x_{21}, z's) + \theta(x_{21} - x_{20}) G(x_{20}, z's). \tag{99}$$

This function can be easily found using the analytic solution (13) for the asymptotics of G and Γ at high energies.

The initial conditions for the scalar functions G_2 and Γ_2 in Eqs. (98) follow from Eq. (93):

$$G_2^{(0)}(x_{10}^2, z) = \Gamma_2^{(0)}(x_{10}^2, x_{21}^2, z') = -\frac{\alpha_s^2 C_F}{N_c} \pi \ln \frac{1}{x_{10} \Lambda}. \tag{100}$$

It is useful to check that the transverse coordinate integral in the LLA kernel of Eqs. (98) (the first two lines of (98a) and (98b)) is convergent. To see this, let us use Eq. (99) and Eq. (13) in Eqs. (98), to check the behavior of the integrands in the $x_{21}^2 \gg x_{10}^2$ and $x_{21}^2 \ll x_{10}^2$ limits. Although individual terms appear to be logarithmically divergent in the IR, the sum of the terms scales as

$$\int \frac{dx_{21}^2}{(x_{21}^2)^{1.5-\alpha_h^q}} \ln \frac{1}{x_{21}^2 \Lambda^2}, \tag{101}$$

which is convergent for $\alpha_h^q < \frac{1}{2}$. Noting from Eq. (14) that $\alpha_h^q \sim \sqrt{\alpha_s} \ll 1$, we conclude that this integral is convergent in the IR for perturbative α_s . In the UV, the terms converge as

$$\int_0 dx_{21}^2 \ln \frac{1}{x_{21}^2 \Lambda^2} (x_{21}^2)^c \alpha_h^q \tag{102}$$

with c a positive constant depending on the term. We therefore conclude that the transverse coordinate integral in Eqs. (98) is convergent in both the UV and IR limits.

The most intricate part of Eqs. (98) is the treatment of the non-logarithmic transverse integral; we want to evaluate

it as completely as possible within our DLA accuracy. Focusing on the evolution of G_2 in Eq. (98a), that integral is

$$J \equiv \frac{\alpha_s N_c}{2\pi^2} \int_{\frac{\Lambda^2}{s}}^z \frac{dz'}{z'} \int d^2x_2 \ln \frac{1}{x_{21}^2 \Lambda^2} \frac{x_{10} \cdot x_{21}}{x_{10}^2 x_{21}^2} \left[\Gamma_{gen}(x_{20}^2, x_{21}^2, z's) + G(x_{21}^2, z's) \right] \\ - \frac{\alpha_s N_c}{2\pi^2} \int_{\frac{\Lambda^2}{s}}^z \frac{dz'}{z'} \int d^2x_2 \ln \frac{1}{x_{21}^2 \Lambda^2} \frac{x_{10} \cdot x_{20}}{x_{10}^2 x_{20}^2} \left[\Gamma_{gen}(x_{20}^2, x_{21}^2, z's) + \Gamma_{gen}(x_{21}^2, x_{20}^2, z's) \right]. \quad (103)$$

Next we insert the expression (99) for Γ_{gen} and the asymptotic solutions (13), scaling out the various power-counting parameters:

$$J = \frac{\alpha_s N_c}{2\pi^2} \int_{\frac{\Lambda^2}{s}}^z \frac{dz'}{z'} (z's x_{10}^2)^{\alpha_h^q} G_0 j(x_{10}^2) = \left(\frac{\alpha_s N_c}{2\pi^2} \frac{1}{\alpha_h^q} G_0 \right) j(x_{10}^2) (zs x_{10}^2)^{\alpha_h^q}, \quad (104)$$

where

$$j(x_{10}^2) \equiv \frac{1}{G_0} \int d^2x_2 \ln \frac{1}{x_{21}^2 \Lambda^2} (z's x_{10}^2)^{-\alpha_h^q} \\ \times \left\{ \frac{x_{10}}{x_{10}^2} \cdot \left(\frac{x_{21}}{x_{21}^2} - \frac{x_{20}}{x_{20}^2} \right) \left[\theta(x_{21}^2 - x_{20}^2) G(x_{20}^2, z's) + \theta(x_{20}^2 - x_{21}^2) \Gamma(x_{20}^2, x_{21}^2, z's) \right] \right. \\ \left. - \left(\frac{x_{10} \cdot x_{20}}{x_{10}^2 x_{20}^2} \right) \left[\theta(x_{20}^2 - x_{21}^2) G(x_{21}^2, z's) + \theta(x_{21}^2 - x_{20}^2) \Gamma(x_{21}^2, x_{20}^2, z's) \right] \right. \\ \left. + \left(\frac{x_{10} \cdot x_{21}}{x_{10}^2 x_{21}^2} \right) G(x_{21}^2, z's) \right\}. \quad (105)$$

Using the expressions in (13) we write

$$j(x_{10}^2) = \frac{1}{3} \int d^2x_2 \ln \frac{1}{x_{21}^2 \Lambda^2} \\ \times \left\{ \frac{x_{10}}{x_{10}^2} \cdot \left(\frac{x_{21}}{x_{21}^2} - \frac{x_{20}}{x_{20}^2} \right) \left[\theta(x_{21}^2 - x_{20}^2) \left(\frac{x_{20}^2}{x_{10}^2} \right)^{\alpha_h^q} + \theta(x_{20}^2 - x_{21}^2) \left(\frac{x_{21}^2}{x_{10}^2} \right)^{\alpha_h^q} \left(4 \left(\frac{x_{20}^2}{x_{21}^2} \right)^{\frac{\alpha_h^q}{4}} - 3 \right) \right] \right. \\ \left. - \left(\frac{x_{10} \cdot x_{20}}{x_{10}^2 x_{20}^2} \right) \left[\theta(x_{20}^2 - x_{21}^2) \left(\frac{x_{21}^2}{x_{10}^2} \right)^{\alpha_h^q} + \theta(x_{21}^2 - x_{20}^2) \left(\frac{x_{20}^2}{x_{10}^2} \right)^{\alpha_h^q} \left(4 \left(\frac{x_{21}^2}{x_{20}^2} \right)^{\frac{\alpha_h^q}{4}} - 3 \right) \right] \right. \\ \left. + \left(\frac{x_{10} \cdot x_{21}}{x_{10}^2 x_{21}^2} \right) \left(\frac{x_{21}^2}{x_{10}^2} \right)^{\alpha_h^q} \right\}. \quad (106)$$

Consider the DLA power counting in Eq. (104). This step of evolution contains an explicit factor of α_s , together with $\frac{1}{\alpha_h^q}$ and G_0 . From Eq. (14) we see that $\frac{1}{\alpha_h^q} \sim \frac{1}{\sqrt{\alpha_s}}$, and from Eq. (94), we see that the scaling initial conditions G_0 contain a relative logarithm of energy, which also scales as $\frac{1}{\sqrt{\alpha_s}}$ in the DLA power counting ($\alpha_s \ln^2 \frac{s}{\Lambda^2} \sim 1$ such that $\ln \frac{s}{\Lambda^2} \sim \frac{1}{\sqrt{\alpha_s}}$). The factor in parentheses in (104) is therefore an $\mathcal{O}(1)$ step of evolution in this limit, and the energy dependence $(zs x_{10}^2)^{\alpha_h^q}$ is also an $\mathcal{O}(1)$ resummation. Next we note that the quantity $j(x_{10}^2)$ in Eq. (105) is independent of the energy $z's$, is a dimensionless function of x_{10} and Λ , and converges in the IR, such that the IR cutoff Λ enters only in a single logarithm in the integrand. Therefore, the general form of $j(x_{10}^2)$ can be written as

$$j(x_{10}^2) = f_1(\alpha_s) \ln \frac{1}{x_{10} \Lambda} + f_2(\alpha_s), \quad (107)$$

where f_1 and f_2 are some functions only of α_s and contain no additional logarithms of energy or of x_{10} . The residual α_s dependence in f_1 and f_2 is thus not enhanced by any logarithms and only contributes to higher-order non-logarithmic corrections. In this spirit we therefore set $\alpha_s \rightarrow 0$ in Eq. (105), replacing both G and Γ from (13) by $\frac{1}{3}G_0$, obtaining

$$j(x_{10}^2) = \frac{2}{3} \int d^2x_2 \ln \frac{1}{x_{21}^2 \Lambda^2} \frac{x_{10}}{x_{10}^2} \cdot \left(\frac{x_{21}}{x_{21}^2} - \frac{x_{20}}{x_{20}^2} \right). \quad (108)$$

The integral now is at most log-divergent in x_{21} , and even that divergence is zero after the angular integrations. Writing $d^2x_2 = x_{21}dx_{21}d\phi$ we can eliminate the first term in parentheses after the angular averaging.⁶ Angular integration in the second term gives (see Eq. (A.14) of [47])

$$j(x_{10}^2) = -\frac{4\pi}{3} \frac{1}{x_{10}^2} \int_0^\infty dx_{21} x_{21} \ln \frac{1}{x_{21}^2 \Lambda^2} \theta(x_{10} - x_{21}) = -\frac{4\pi}{3} \ln \frac{1}{x_{10} \Lambda} - \frac{2\pi}{3}. \quad (109)$$

Neglecting the constant compared to the logarithm and substituting our result back into Eq. (104) we arrive at

$$J = -\left(\frac{\alpha_s N_c}{3\pi} \frac{1}{\alpha_h^q} G_0 \right) (zs x_{10}^2)^{\alpha_h^q} \ln \frac{1}{x_{10}^2 \Lambda^2}. \quad (110)$$

Employing Eq. (110) in Eqs. (98) to replace the terms containing Γ_{gen} and G yields

$$\begin{aligned} G_2(x_{10}^2, zs) &= G_2^{(0)}(x_{10}^2, zs) - \left(\frac{\alpha_s N_c}{3\pi} \frac{1}{\alpha_h^q} G_0 \right) (zs x_{10}^2)^{\alpha_h^q} \ln \frac{1}{x_{10}^2 \Lambda^2} \\ &\quad - \frac{\alpha_s N_c}{2\pi} \int_{\frac{1}{x_{10}^2 s}}^z \frac{dz'}{z'} \int_{\frac{1}{z' s}}^{x_{10}^2} \frac{dx_{21}^2}{x_{21}^2} \Gamma_2(x_{10}^2, x_{21}^2, z' s), \end{aligned} \quad (111a)$$

$$\begin{aligned} \Gamma_2(x_{10}^2, x_{21}^2, z' s) &= G_2^{(0)}(x_{10}^2, z' s) - \left(\frac{\alpha_s N_c}{3\pi} \frac{1}{\alpha_h^q} G_0 \right) (z' s x_{10}^2)^{\alpha_h^q} \ln \frac{1}{x_{10}^2 \Lambda^2} \\ &\quad - \frac{\alpha_s N_c}{2\pi} \int_{\frac{1}{x_{10}^2 s}}^{z'} \frac{dz''}{z''} \int_{\frac{1}{z'' s}}^{\min[x_{10}^2, x_{21}^2 \frac{z'}{z''}]} \frac{dx_{31}^2}{x_{31}^2} \Gamma_2(x_{10}^2, x_{31}^2, z'' s). \end{aligned} \quad (111b)$$

This leaves the simplified equations (111) amenable to analytic solution, which we will pursue next.

B. High-Energy Asymptotics

To begin, it is convenient to rescale the functions G_2 and Γ_2 to eliminate the constants:

$$G_2 \equiv \left(-\frac{\alpha_s N_c}{3\pi} \frac{1}{\alpha_h^q} G_0 \ln \frac{1}{x_{10}^2 \Lambda^2} \right) \bar{G}_2 = \left(-\frac{G_0}{2\sqrt{3}} \sqrt{\frac{\alpha_s N_c}{2\pi}} \ln \frac{1}{x_{10}^2 \Lambda^2} \right) \bar{G}_2, \quad (112a)$$

$$\Gamma_2 \equiv \left(-\frac{\alpha_s N_c}{3\pi} \frac{1}{\alpha_h^q} G_0 \ln \frac{1}{x_{10}^2 \Lambda^2} \right) \bar{\Gamma}_2 = \left(-\frac{G_0}{2\sqrt{3}} \sqrt{\frac{\alpha_s N_c}{2\pi}} \ln \frac{1}{x_{10}^2 \Lambda^2} \right) \bar{\Gamma}_2, \quad (112b)$$

which casts Eq. (111) into the form

$$\bar{G}_2(x_{10}^2, zs) = (zs x_{10}^2)^{\alpha_h^q} - \frac{\alpha_s N_c}{2\pi} \int_{\frac{1}{x_{10}^2 s}}^z \frac{dz'}{z'} \int_{\frac{1}{z' s}}^{x_{10}^2} \frac{dx_{21}^2}{x_{21}^2} \bar{\Gamma}_2(x_{10}^2, x_{21}^2, z' s), \quad (113a)$$

$$\bar{\Gamma}_2(x_{10}^2, x_{21}^2, z' s) = (z' s x_{10}^2)^{\alpha_h^q} - \frac{\alpha_s N_c}{2\pi} \int_{\frac{1}{x_{10}^2 s}}^{z'} \frac{dz''}{z''} \int_{\frac{1}{z'' s}}^{\min[x_{10}^2, x_{21}^2 \frac{z'}{z''}]} \frac{dx_{31}^2}{x_{31}^2} \bar{\Gamma}_2(x_{10}^2, x_{31}^2, z'' s), \quad (113b)$$

⁶ It appears important to first choose the integration variables for the whole integral, and then integrate both terms in parenthesis using the same variables. If one simply discards the first term in parentheses, and writes $d^2x_2 = x_{20}dx_{20}d\phi'$ for the second term, the result appears to be IR divergent again due to an illegal variable shift in one of two divergent terms of an overall convergent integral.

where we have neglected the initial conditions for G_2 and Γ_2 as small when compared to the J -term from Eq. (110). Introducing the logarithmic variables

$$\eta \equiv \sqrt{\frac{\alpha_s N_c}{2\pi}} \ln \frac{zs}{\Lambda^2}, \quad s_{10} \equiv \sqrt{\frac{\alpha_s N_c}{2\pi}} \ln \frac{1}{x_{10}^2 \Lambda^2}, \quad (114a)$$

$$\eta' \equiv \sqrt{\frac{\alpha_s N_c}{2\pi}} \ln \frac{z's}{\Lambda^2}, \quad s_{21} \equiv \sqrt{\frac{\alpha_s N_c}{2\pi}} \ln \frac{1}{x_{21}^2 \Lambda^2}, \quad (114b)$$

$$\eta'' \equiv \sqrt{\frac{\alpha_s N_c}{2\pi}} \ln \frac{z''s}{\Lambda^2}, \quad s_{31} \equiv \sqrt{\frac{\alpha_s N_c}{2\pi}} \ln \frac{1}{x_{31}^2 \Lambda^2}, \quad (114c)$$

along with the scaling variables

$$\chi \equiv \eta - s_{10} = \sqrt{\frac{\alpha_s N_c}{2\pi}} \ln(zs x_{10}^2), \quad (115a)$$

$$\zeta \equiv \eta' - s_{10} = \sqrt{\frac{\alpha_s N_c}{2\pi}} \ln(z's x_{10}^2), \quad \zeta' \equiv \eta' - s_{21} = \sqrt{\frac{\alpha_s N_c}{2\pi}} \ln(z's x_{21}^2), \quad (115b)$$

$$\xi \equiv \eta'' - s_{10} = \sqrt{\frac{\alpha_s N_c}{2\pi}} \ln(z''s x_{10}^2), \quad \xi' \equiv \eta'' - s_{31} = \sqrt{\frac{\alpha_s N_c}{2\pi}} \ln(z''s x_{31}^2), \quad (115c)$$

and the rescaled intercept as $\hat{\alpha}_h^q \equiv \frac{4}{\sqrt{3}}$, we can rewrite Eqs. (113) in the simple form

$$\bar{G}_2(\chi) = e^{\hat{\alpha}_h^q \chi} - \int_0^\chi d\zeta \int_0^\zeta d\zeta' \bar{\Gamma}_2(\zeta, \zeta'), \quad (116a)$$

$$\bar{\Gamma}_2(\zeta, \zeta') = e^{\hat{\alpha}_h^q \zeta} - \int_0^{\zeta'} d\xi \int_0^\xi d\xi' \bar{\Gamma}_2(\xi, \xi') - \int_{\zeta'}^\zeta d\xi \int_0^{\zeta'} d\xi' \bar{\Gamma}_2(\xi, \xi'). \quad (116b)$$

Let us emphasize that, although we have expressed Eqs. (116) in terms of scaling variables, we have not imposed a scaling form on the functions, rather it resulted naturally from the form of the equations.

Following the procedure used in [39] to obtain an analytic solution for the quark helicity distribution, we first differentiate Eqs. (116) to get

$$\frac{\partial}{\partial \chi} \bar{G}_2(\chi) = \hat{\alpha}_h^q e^{\hat{\alpha}_h^q \chi} - \int_0^\chi d\zeta' \bar{\Gamma}_2(\chi, \zeta'), \quad (117a)$$

$$\frac{\partial}{\partial \zeta} \bar{\Gamma}_2(\zeta, \zeta') = \hat{\alpha}_h^q e^{\hat{\alpha}_h^q \zeta} - \int_0^{\zeta'} d\xi' \bar{\Gamma}_2(\zeta, \xi'), \quad (117b)$$

with the boundary condition

$$\bar{\Gamma}_2(\zeta', \zeta') = \bar{G}_2(\zeta'). \quad (118)$$

Next, we introduce the Laplace transforms

$$\bar{G}_2(\chi) = \int \frac{d\omega}{2\pi i} e^{\omega \chi} \bar{G}_{2\omega}, \quad \bar{\Gamma}_2(\zeta, \zeta') = \int \frac{d\omega}{2\pi i} e^{\omega \zeta'} \bar{\Gamma}_{2\omega}(\zeta), \quad (119a)$$

$$\bar{G}_{2\omega} = \int_0^\infty d\chi e^{-\omega \chi} \bar{G}_2(\chi), \quad \bar{\Gamma}_{2\omega}(\zeta) = \int_0^\infty d\zeta' e^{-\omega \zeta'} \bar{\Gamma}_2(\zeta, \zeta'), \quad (119b)$$

and start by focusing on Eq. (117b), obtaining

$$\frac{\partial}{\partial \zeta} \bar{\Gamma}_{2\omega}(\zeta) = \frac{\hat{\alpha}_h^q}{\omega} e^{\hat{\alpha}_h^q \zeta} - \frac{1}{\omega} \bar{\Gamma}_{2\omega}(\zeta). \quad (120)$$

This ODE is straightforward to solve, and the solution reads

$$\bar{\Gamma}_{2\omega}(\zeta) = \frac{\hat{\alpha}_h^q}{1 + \hat{\alpha}_h^q \omega} e^{\hat{\alpha}_h^q \zeta} + \hat{\alpha}_h^q C_\omega e^{-\frac{\zeta}{\omega}} \quad (121)$$

with the integration “constant” C_ω , such that

$$\bar{\Gamma}_2(\zeta, \zeta') = \int \frac{d\omega}{2\pi i} e^{\omega \zeta'} \left[\frac{\hat{\alpha}_h^q}{1 + \hat{\alpha}_h^q \omega} e^{\hat{\alpha}_h^q \zeta} + \hat{\alpha}_h^q C_\omega e^{-\frac{\zeta}{\omega}} \right]. \quad (122)$$

Collecting the pole at $\omega = -\frac{1}{\hat{\alpha}_h^q}$ and using the boundary condition (118) to obtain the corresponding solution for G , we have

$$\bar{G}_2(\chi) = e^{\left(\hat{\alpha}_h^q - \frac{1}{\hat{\alpha}_h^q}\right)\chi} + \int \frac{d\omega}{2\pi i} \hat{\alpha}_h^q C_\omega e^{(\omega - \frac{1}{\omega})\chi}, \quad (123a)$$

$$\bar{\Gamma}_2(\zeta, \zeta') = e^{\hat{\alpha}_h^q \zeta - \frac{1}{\hat{\alpha}_h^q} \zeta'} + \int \frac{d\omega}{2\pi i} \hat{\alpha}_h^q C_\omega e^{\omega \zeta' - \frac{\zeta}{\omega}}. \quad (123b)$$

The integration constants C_ω can be constrained by back-substituting the solution (123) into the differential equations (117). Plugging Eq. (123b) into Eq. (117b) we arrive at the condition

$$\int \frac{d\omega}{2\pi i} \frac{1}{\omega} C_\omega e^{-\frac{\zeta}{\omega}} = 0, \quad (124)$$

and similarly, using Eq. (123a) in Eq. (117a), we obtain

$$\int \frac{d\omega}{2\pi i} \omega C_\omega e^{(\omega - \frac{1}{\omega})\zeta} = \frac{1}{(\hat{\alpha}_h^q)^2} e^{\left(\hat{\alpha}_h^q - \frac{1}{\hat{\alpha}_h^q}\right)\zeta}. \quad (125)$$

This equation is hard to solve exactly, but it is straightforward to match the large- ζ asymptotics. In Eq. (125), there is a pole at $\omega = 0$ in the exponent which can be shown to give a contribution that asymptotes to zero as $\zeta \rightarrow \infty$ (see Appendix A for the calculation). Hence, to make Eq. (125) be valid at $\zeta \rightarrow \infty$, we simply need C_ω to contain a pole $\omega = \hat{\alpha}_h^q$, with an appropriate choice of the coefficient:

$$C_\omega = \frac{1}{(\hat{\alpha}_h^q)^3} \frac{1}{\omega - \hat{\alpha}_h^q}. \quad (126)$$

We verify explicitly in Appendix A that Eq. (126) solves Eq. (125) in the large- ζ asymptotics and that the $\omega = 0$ pole is suppressed.

The asymptotic solution to Eqs. (116) is thus (using $\hat{\alpha}_h^q = \frac{4}{\sqrt{3}}$)

$$\bar{G}_2(\chi \gg 1) = \left(1 + \frac{1}{(\hat{\alpha}_h^q)^2}\right) e^{\left(\hat{\alpha}_h^q - \frac{1}{\hat{\alpha}_h^q}\right)\chi} = \frac{19}{16} e^{\frac{13}{4\sqrt{3}}\chi}, \quad (127a)$$

$$\bar{\Gamma}_2(\zeta \gg 1, \zeta' \gg 1) = e^{\hat{\alpha}_h^q \zeta - \frac{\zeta'}{\hat{\alpha}_h^q}} + \frac{1}{(\hat{\alpha}_h^q)^2} e^{\hat{\alpha}_h^q \zeta' - \frac{\zeta}{\hat{\alpha}_h^q}} = e^{\frac{4}{\sqrt{3}}\zeta - \frac{\sqrt{3}}{4}\zeta'} + \frac{3}{16} e^{\frac{4}{\sqrt{3}}\zeta' - \frac{\sqrt{3}}{4}\zeta}. \quad (127b)$$

Our analytic solution can be cross-checked numerically. We did this by solving Eqs. (116) on a discretized grid, exactly analogous to what we did in Ref. [38]. The resulting numerical solution of \bar{G}_2 is shown in Fig. 7 for a grid spacing of 0.033.⁷ These curves demonstrate the scaling behavior of \bar{G}_2 in agreement with our analytic result in Eq. (127a). Moreover, from the slope of this curve we find agreement with the exponent $13/(4\sqrt{3})$ of \bar{G}_2 to within 1%.

To cross-check our solution for $\bar{\Gamma}_2$ we take the ratio of Eqs. (127b) and (127a) to obtain

$$\frac{\bar{\Gamma}_2(\zeta, \zeta')}{\bar{G}_2(\zeta)} = \frac{16}{19} \left[e^{\frac{\zeta - \zeta'}{\hat{\alpha}_h^q}} + \frac{1}{(\hat{\alpha}_h^q)^2} e^{\hat{\alpha}_h^q (\zeta' - \zeta)} \right] = \frac{16}{19} \left[e^{\frac{\sqrt{3}}{4} (s_{21} - s_{10})} + \frac{3}{16} e^{-\frac{4}{\sqrt{3}} (s_{21} - s_{10})} \right]. \quad (128)$$

⁷ This corresponds to using maximum η and s values (see Eqs. (114)) of 10 with a grid size of 300.

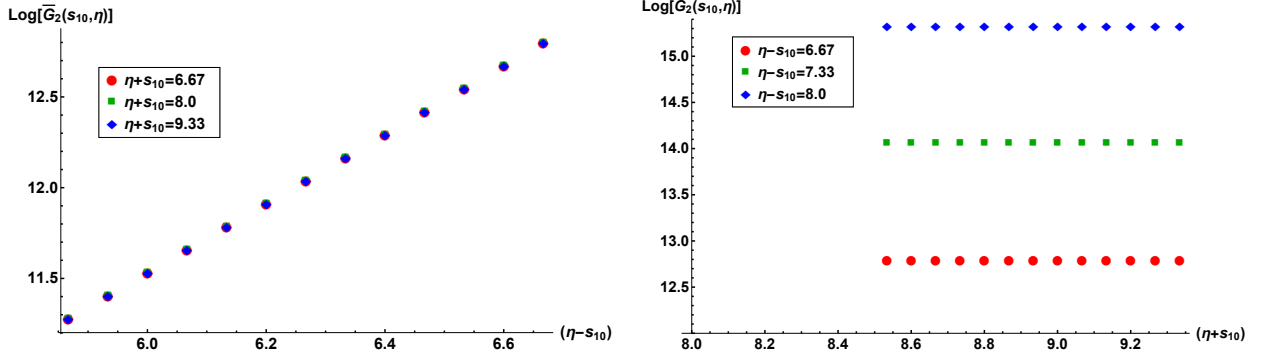


FIG. 7. Numerical solution of Eqs. (116) for $\ln \bar{G}_2$ plotted as a function of $\eta - s_{10}$ (for three different values of $\eta + s_{10}$) in the left panel and as a function of $\eta + s_{10}$ (for three different values of $\eta - s_{10}$) in the right panel. Both panels demonstrate that \bar{G}_2 is only a function of $\eta - s_{10}$, as expected from Eq. (127a).

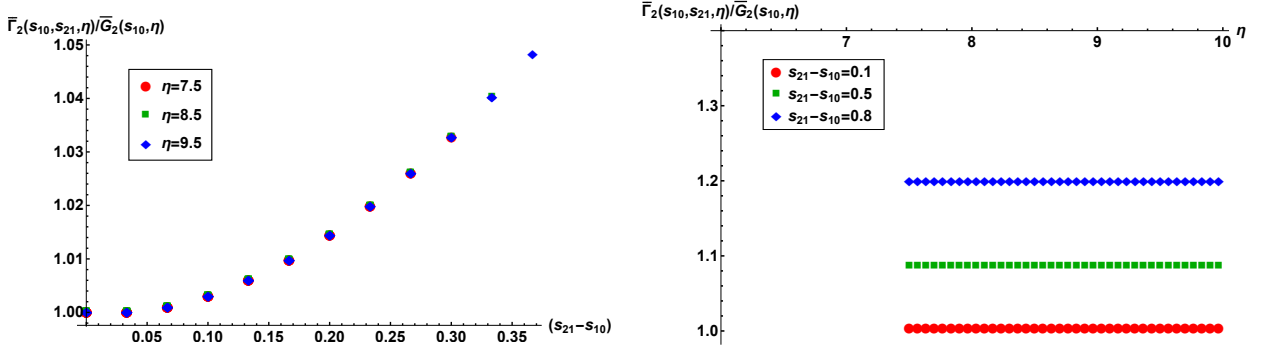


FIG. 8. Plot of the $\bar{\Gamma}_2/\bar{G}_2$ ratio given by the numerical solution of Eqs. (116) as a function of $s_{21} - s_{10}$ (for three different values of η) in the left panel and as a function of η (for three different values of $s_{21} - s_{10}$) in the right panel. Both panels demonstrate that $\bar{\Gamma}_2/\bar{G}_2$ is only a function of $s_{21} - s_{10}$ in agreement with Eq. (128).

The ratio $\bar{\Gamma}_2/\bar{G}_2$ given by our numerical solution is shown in Fig. 8. The plots demonstrate that the ratio $\bar{\Gamma}_2/\bar{G}_2$ is only a function of $s_{21} - s_{10}$, in agreement with our analytical result (128). We likewise were able to confirm in the physical region $s_{10} < s_{21} < \eta$ the functional form of (128), where we found agreement with the exponent $\sqrt{3}/4$ to within 5% and the coefficient $16/19$ to within $< 0.5\%$. Thus, we have numerically confirmed our analytic solution for both \bar{G}_2 and $\bar{\Gamma}_2$.

Finally, converting Eqs. (127) back into the standard variables by using Eqs. (115) and reinserting the scaling factors from Eq. (112) gives us our final answer

$$G_2(x_{10}^2, zs) \approx -\frac{19}{32\sqrt{3}} \sqrt{\frac{\alpha_s N_c}{2\pi}} G_0 \ln \frac{1}{x_{10}^2 \Lambda^2} (zs x_{10}^2)^{\frac{13}{4\sqrt{3}}} \sqrt{\frac{\alpha_s N_c}{2\pi}}, \quad (129a)$$

$$\Gamma_2(x_{10}^2, x_{21}^2, z's) \approx -\frac{1}{2\sqrt{3}} \sqrt{\frac{\alpha_s N_c}{2\pi}} G_0 \ln \frac{1}{x_{10}^2 \Lambda^2} \left[(z's x_{10}^2)^{\frac{4}{\sqrt{3}}} \sqrt{\frac{\alpha_s N_c}{2\pi}} (z's x_{21}^2)^{-\frac{\sqrt{3}}{4}} \sqrt{\frac{\alpha_s N_c}{2\pi}} \right. \\ \left. + \frac{3}{16} (z's x_{21}^2)^{\frac{4}{\sqrt{3}}} \sqrt{\frac{\alpha_s N_c}{2\pi}} (z's x_{10}^2)^{-\frac{\sqrt{3}}{4}} \sqrt{\frac{\alpha_s N_c}{2\pi}} \right]. \quad (129b)$$

The asymptotic solution (129a) for the polarized dipole amplitude G_2 is the central result of this work. Substituting

the solution Eq. (129a) into Eq. (41) yields the small- x asymptotics of the dipole gluon helicity distribution:

$$g_{1L}^{G dip}(x, k_T^2) \sim G_2(x_{10}^2, zs = \frac{Q^2}{x}) \sim \left(\frac{1}{x}\right)^{\alpha_h^G} \quad (130)$$

with the gluon helicity intercept

$$\alpha_h^G = \frac{13}{4\sqrt{3}} \sqrt{\frac{\alpha_s N_c}{2\pi}} \approx 1.88 \sqrt{\frac{\alpha_s N_c}{2\pi}}. \quad (131)$$

Strictly speaking, this intercept has been obtained by solving the small- x evolution equations (96) applicable to the dipole gluon helicity distribution (41). The Weizsäcker-Williams gluon helicity distribution (51) is defined by a different operator (52) than the dipole gluon helicity distribution (37), and in general will have different evolution equations than (96). While we leave the derivation and solution of these evolution equations for future work, we note that both the dipole and WW gluon helicity TMDs must give the same gluon helicity PDF ΔG when integrated over all k_T . Integrating Eqs. (41) and (51) over the transverse momentum to obtain the collinear gluon helicity distribution ΔG , we confirm that both distributions reduce to a common operator, and that all three distributions possess the same small- x asymptotics:

$$\begin{aligned} \Delta G(x, Q^2) &= \int d^2k g_{1L}^{G WW}(x, k_T^2) = \int d^2k g_{1L}^{G dip}(x, k_T^2) \\ &= \frac{1}{\alpha_s 2\pi^2} \int d^2x_0 \epsilon_T^{ij} \left\langle \text{tr} \left[(V_0^{pol})^\perp_i \left(\frac{\partial}{\partial(x_0)^\perp_j} V_0^\dagger \right) \right] + \text{c.c.} \right\rangle \\ &= \frac{-2N_c}{\alpha_s \pi^2} \left[\left(1 + x_{10}^2 \frac{\partial}{\partial x_{10}^2} \right) G_2(x_{10}^2, zs = \frac{Q^2}{x}) \right]_{x_{10}^2 = \frac{1}{Q^2}}. \end{aligned} \quad (132)$$

We conclude that

$$\Delta G(x, Q^2) \sim \left(\frac{1}{x}\right)^{\alpha_h^G} \sim \left(\frac{1}{x}\right)^{\frac{13}{4\sqrt{3}} \sqrt{\frac{\alpha_s N_c}{2\pi}}} \sim \left(\frac{1}{x}\right)^{1.88 \sqrt{\frac{\alpha_s N_c}{2\pi}}}. \quad (133)$$

Thus, we see that the small- x asymptotics of these three distributions ($\Delta G, g_{1L}^{G dip}, g_{1L}^{G WW}$) – and, indeed, *all* possible definitions of gluon helicity TMDs – are universal and governed by the gluon helicity intercept (131).

VI. PHENOMENOLOGY OF THE GLUON SPIN AT SMALL x

In this section we give an estimate for the gluon spin S_G in (1) based on our gluon helicity intercept (131). The gluon spin has been a topic of intense investigation, with only recent experiments showing that it can give a more substantial fraction of the proton's spin than once thought [62, 63]. Nevertheless, the estimates of S_G are still plagued by the lack of data below $x = 0.05$, which causes large uncertainties in this quantity (see, e.g., Ref. [64]), and is one of the main motivations for the construction of an Electron-Ion Collider. However, we emphasize that once our theoretical calculations of the gluon (and quark) helicity intercepts push beyond the current approximations and include, e.g., large- N_c & N_f , running coupling, and LLA corrections, one could use these results in future extractions of the already existing data to provide strong constraints on the small- x behavior of the helicity PDFs, and, consequently, the quark and gluon spin. (We mention that helicity PDFs have been extracted by several groups, e.g., DSSV [43, 65], JAM [66–68], LSS [69–71], NNPDF [72, 73].)

In order to calculate S_G , we need input for the gluon helicity PDF $\Delta G(x, Q^2)$, and we focus here on the fit from DSSV14 [43]. We proceed through a simple approach, which we also employed in Ref. [38] for an estimate of the quark spin based on (3), and leave a more rigorous phenomenological study for future work. First, we attach a curve $\Delta \tilde{G}(x, Q^2) = N x^{-\alpha_h^G}$ (with α_h^G given in (131)) to the DSSV14 result for $\Delta G(x, Q^2)$ at a particular small- x point x_0 . We fix the normalization N by requiring $\Delta \tilde{G}(x_0, Q^2) = \Delta G(x_0, Q^2)$. Then we calculate the truncated integral

$$S_G^{[x_{min}]}(Q^2) \equiv \int_{x_{min}}^1 dx \Delta G(x, Q^2) \quad (134)$$

of the modified gluon helicity PDF

$$\Delta G_{mod}(x, Q^2) \equiv \theta(x - x_0) \Delta G(x, Q^2) + \theta(x_0 - x) \Delta \tilde{G}(x, Q^2) \quad (135)$$

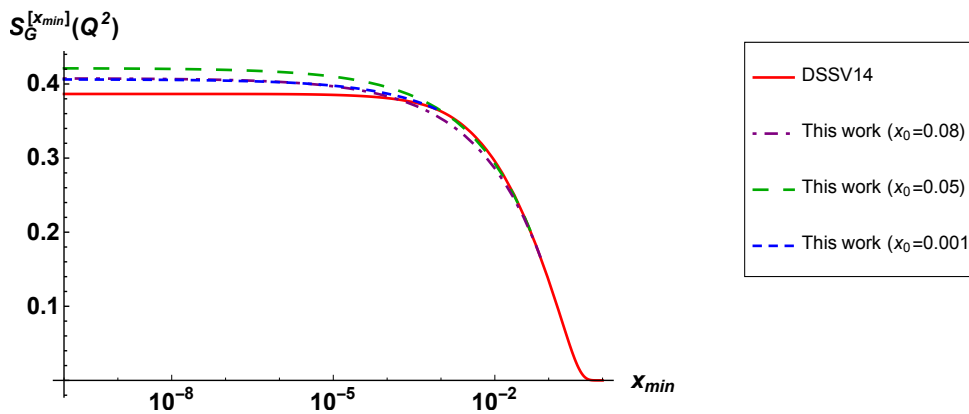


FIG. 9. Plot of $S_G^{[x_{min}]}(Q^2)$ vs. x_{min} at $Q^2 = 10 \text{ GeV}^2$. The solid curve is from DSSV14 [43]. The dot-dashed, long-dashed, and short-dashed curves are from various small- x modifications of $\Delta G(x, Q^2)$ at $x_0 = 0.08, 0.05, 0.001$, respectively, using our gluon helicity intercept (see the text for details).

for different x_0 values. The results are shown in Fig. 9 for $Q^2 = 10 \text{ GeV}^2$ and $\alpha_s \approx 0.25$, in which case $\alpha_h^G \approx 0.65$. We see that the small- x evolution of $\Delta G(x, Q^2)$ gives about a $5 \div 10\%$ increase to the gluon spin, depending on where in x the effects set in and on the parameterization of the gluon helicity PDF at higher x . Again we emphasize that the first principles results of this work (along with that for the quark [9, 38, 39]) can be included in future extractions of helicity PDFs, especially once the present large- N_c approximation is relaxed, which will provide strong constraints on the small- x behavior of the quark and gluon spin.

Saturation effects may also impact the amount of spin carried by small- x quarks and gluons. The small- x asymptotics of ΔG found here and the small- x asymptotics of Δq found in [9, 38, 39] are such that $x\Delta G \rightarrow 0$ and $x\Delta q \rightarrow 0$ as $x \rightarrow 0$. Hence the helicity PDFs will not violate unitarity at small x . However, as one can see from the helicity evolution equations including (LLA) saturation effects, as derived in [9, 37], saturation would completely suppress the small- x evolution of helicity PDFs, making the effective α_h^q and α_h^G zero in the saturation region (cf. [26] for the flavor non-singlet unpolarized quark distribution). Therefore, a very small amount of the proton spin should reside in the saturation region. This observation can become an important component of the future small- x helicity PDF phenomenology.

VII. CONCLUSIONS

In this paper, we have shown that the dipole gluon helicity distribution (40) and the Weizsäcker-Williams gluon helicity distribution (54) at small x are governed by polarized dipole operators (37) and (52), respectively. These operators are different from each other and from the polarized dipole amplitude (8) which governs the quark helicity distribution at small x . For the case of the dipole gluon helicity distribution, we have derived double-logarithmic small- x evolution equations given by Eqs. (96) in the large- N_c limit. These gluon helicity evolution equations mix with the small- x quark helicity evolution (13), but ultimately result in a gluon helicity intercept (131) which is smaller than the quark helicity intercept (14) by about 20%. One may speculate that the fact that $\alpha_h^G < \alpha_h^q$ is partially responsible for the difficulty in experimentally detecting a non-zero signal for ΔG at small- x .

The difference between the quark and gluon helicity intercepts mathematically results from the fact that the small- x evolution for quark and gluon helicity is given by a coupled set of equations, Eqs. (12) and (96). This is similar to the Dokshitzer-Gribov-Lipatov-Altarelli-Parisi (DGLAP) evolution equations [74–76] which mix the evolution of the (flavor-singlet) quark and gluon distributions. Due to this mixing, the Q^2 dependence of quark and gluon PDFs is different from each other. The unpolarized small- x evolution is different in this respect: at LLA the BFKL evolution is entirely gluon-driven. The quark distribution is obtained from this evolution by having a gluon at the end of BFKL ladder emit a $q\bar{q}$ pair. This results in x -dependence of the (flavor-singlet) unpolarized quark distribution at small x being practically the same as that for the gluons. In this paper we observed that for helicity TMDs and PDFs the small- x evolution mixes the contributions of quarks and gluons, resulting in a different x -dependence of quark and gluon helicity PDFs. This is indeed different from the x -dependence of unpolarized quark and gluon PDFs resulting from BFKL evolution.

On a technical level, this reduction of the gluon helicity as compared to the quark helicity can be attributed to the fact that the dipole gluon helicity evolution receives contributions from the radiation of virtual unpolarized

gluons, but not real unpolarized gluons (the bottom two diagrams of Fig. 5). The physical reason for this stems from the definition (23) of what gluon helicity really means: a circular flow of the gluon field-strength. Maintaining this circular orientation during the small- x evolution requires that the angular correlations between the fields be preserved, but in the DLA limit, the radiation of unpolarized gluons is isotropic. The resulting angular decorrelation causes the real gluon emission term to drop out from the gluon helicity evolution equations (98), leaving only the virtual emissions. Consequently, this leads to a depletion of the gluon helicity compared to the quark helicity: the uncorrelated radiation of soft gluons causes the gluon distribution to “forget” about polarized interactions which take place later in the cascade. Only cascades which develop without such uncorrelated radiation contribute to the gluon helicity.

The fact that gluon helicity, which relies upon the circular transverse structure of the fields, is capable of decorrelating can also be seen in the structure of the polarized Wilson lines. The polarized Wilson line (34) relevant for the gluon helicity couples to a total derivative: the curl operator applied to the entire Wilson line. This is in contrast to the polarized Wilson line (21) relevant for the quark helicity, which couples to a local derivative: the curl operator applied to a single point in the polarized Wilson line. This operator structure suggests that a polarized interaction at any point in the cascade is sufficient to contribute to the quark helicity, while only those polarized interactions which preserve the angular correlations can contribute to the gluon helicity. Presumably, this fundamental difference between the nature of quark and gluon helicity can be attributed to the fact that the quark helicity (5) is defined as a matrix element of the axial vector current. Until such accuracy that the evolution becomes sensitive to the axial anomaly, the axial vector current which defines the quark helicity is conserved during the evolution; a coupling to the axial vector current anywhere in the evolution is guaranteed to propagate back to contribute to the quark helicity distribution.

We also note that the asymptotic solution (133) is an important input to the proton spin puzzle and a first principles prediction to be tested against phenomenological extractions. The total gluon polarization S_G is far less constrained by experiments than the quark polarization S_q , so this theoretical guidance on how to extrapolate from data at finite x down to $x \rightarrow 0$ can provide a useful estimate of S_G . In Sec. VI we gave such an estimate of this quantity in a simple approach and found it could increase the current DSSV extrapolation by $5 \div 10\%$. We stress again that the results for the small x behavior of the gluon (and quark) from this work should be included in future helicity PDF fits.

Additionally, a recent paper [53] has provided a gauge-invariant definition of the gluon orbital angular momentum operator in terms of Wilson lines at small x . Deriving and solving similar small- x evolution equations for such an operator could provide yet another piece of the proton spin decomposition at small x .

In closing, we must emphasize a note of caution about the precise values of our quark and gluon helicity intercepts: these numerical values are the result of a leading-order DLA resummation at large N_c , and they may receive significant corrections at higher orders in α_s , at finite N_c , and at $N_f \neq 0$. The single-logarithmic corrections, which can include the effects of parton saturation and multiple scattering, may be particularly important. Our calculation is also performed at fixed coupling at this accuracy; to precisely set the scale of α_s , a higher-order calculation is needed. Indeed, we know from the unpolarized sector that running coupling corrections [77–80] play an essential role in slowing down the small- x evolution [81, 82] and bringing the theory in line with experiment [83–85]. As such, while much work remains to be done in the intervening years, the growing pool of spin-related operators whose small- x asymptotics have been calculated represents an important step in developing the theoretical framework needed for a future Electron-Ion Collider.

ACKNOWLEDGMENTS

The authors are grateful to Ian Balitsky for his interest in their work and for a number of helpful questions and suggestions. We also thank R. Sassot and W. Vogelsang for providing us with the parameters and Fortran code of the DSSV14 fit. This material is based upon work supported by the U.S. Department of Energy, Office of Science, Office of Nuclear Physics under Award Number DE-SC0004286 (YK), within the framework of the TMD Topical Collaboration (DP), and DOE Contract No. DE-AC52-06NA25396 (MS). MS received additional support from the U.S. Department of Energy, Office of Science under the DOE Early Career Program.

Appendix A: A Cross-Check

Substituting Eq. (126) into the left-hand side of Eq. (125) we get

$$\begin{aligned}
\int \frac{d\omega}{2\pi i} \omega C_\omega e^{(\omega - \frac{1}{\omega})\zeta} &= \frac{3\sqrt{3}}{64} \int \frac{d\omega}{2\pi i} \omega \frac{e^{(\omega - \frac{1}{\omega})\zeta}}{\omega - \frac{4}{\sqrt{3}}} = \frac{3}{16} e^{\frac{13}{4\sqrt{3}}\zeta} + \frac{3\sqrt{3}}{64} \sum_{n=2}^{\infty} \frac{(-\zeta)^n}{n!} \frac{1}{(n-2)!} \frac{d^{n-2}}{d\omega^{n-2}} \left(\frac{e^{\omega\zeta}}{\omega - \frac{4}{\sqrt{3}}} \right) \Big|_{\omega=0} \\
&= \frac{3}{16} e^{\frac{13}{4\sqrt{3}}\zeta} + \frac{3\sqrt{3}}{64} \sum_{n=2}^{\infty} \frac{(-\zeta)^n}{n!} \frac{1}{(n-2)!} \sum_{m=0}^{n-2} \binom{n-2}{m} \zeta^{n-2-m} (-1)^m m! \left(-\frac{\sqrt{3}}{4} \right)^{m+1} \\
&= \frac{3}{16} e^{\frac{13}{4\sqrt{3}}\zeta} + \frac{3\sqrt{3}}{64} \sum_{n=2}^{\infty} \sum_{m=0}^{n-2} \frac{(-\zeta^2)^{n-1}}{n! (n-2-m)!} \left(\frac{\sqrt{3}}{4\zeta} \right)^m = \left| k = n-2-m \right| \quad (A1) \\
&= \frac{3}{16} e^{\frac{13}{4\sqrt{3}}\zeta} + \frac{3\sqrt{3}}{64} \sum_{n=2}^{\infty} \sum_{k=0}^{n-2} \frac{(-\zeta^2)^{n-1}}{n! k!} \left(\frac{\sqrt{3}}{4\zeta} \right)^{n-2-k} = \frac{3}{16} e^{\frac{13}{4\sqrt{3}}\zeta} + \frac{3\sqrt{3}}{64} \sum_{k=0}^{\infty} \sum_{n=k+2}^{\infty} \frac{(-\zeta^2)^{n-1}}{n! k!} \left(\frac{\sqrt{3}}{4\zeta} \right)^{n-2-k} \\
&= \left| l = n-k-2 \right| = \frac{3}{16} e^{\frac{13}{4\sqrt{3}}\zeta} + \frac{3\sqrt{3}}{64} \sum_{k=0}^{\infty} \sum_{l=0}^{\infty} \frac{(-\zeta^2)^{l+k+1}}{(l+k+2)! k!} \left(\frac{\sqrt{3}}{4\zeta} \right)^l = \frac{3}{16} e^{\frac{13}{4\sqrt{3}}\zeta} - \frac{3\sqrt{3}}{64} \sum_{l=0}^{\infty} \left(-\frac{\sqrt{3}}{4} \right)^l J_{l+2}(2\zeta).
\end{aligned}$$

While the remaining sum cannot be cast in a form of a single function, we can deduce its large- ζ asymptotics:

$$\sum_{l=0}^{\infty} \left(-\frac{\sqrt{3}}{4} \right)^l J_{l+2}(2\zeta) \Big|_{\zeta \rightarrow \infty} \rightarrow \sum_{l=0}^{\infty} \left(-\frac{\sqrt{3}}{4} \right)^l \sqrt{\frac{1}{\pi\zeta}} \cos \left(2\zeta - \frac{\pi l}{2} - \frac{5\pi}{4} \right) \sim \frac{1}{\sqrt{\zeta}} \rightarrow 0. \quad (A2)$$

We conclude that

$$\frac{3\sqrt{3}}{64} \int \frac{d\omega}{2\pi i} \omega \frac{e^{(\omega - \frac{1}{\omega})\zeta}}{\omega - \frac{4}{\sqrt{3}}} = \frac{3}{16} e^{\frac{13}{4\sqrt{3}}\zeta} + \mathcal{O} \left(\frac{1}{\sqrt{\zeta}} \right) \quad (A3)$$

and, hence, Eq. (126) solves Eq. (125) in the large- ζ asymptotics.

-
- [1] A. Accardi, J. Albacete, M. Anselmino, N. Armesto, E. Aschenauer et al., *Electron Ion Collider: The Next QCD Frontier - Understanding the glue that binds us all*, 1212.1701.
 - [2] E. C. Aschenauer et al., *The RHIC Spin Program: Achievements and Future Opportunities*, 1304.0079.
 - [3] E.-C. Aschenauer et al., *The RHIC SPIN Program: Achievements and Future Opportunities*, 1501.01220.
 - [4] E.-C. Aschenauer et al., *The RHIC Cold QCD Plan for 2017 to 2023: A Portal to the EIC*, 1602.03922.
 - [5] R. L. Jaffe and A. Manohar, *The G(1) Problem: Fact and Fantasy on the Spin of the Proton*, *Nucl. Phys.* **B337** (1990) 509–546.
 - [6] X.-D. Ji, *Gauge-Invariant Decomposition of Nucleon Spin*, *Phys. Rev. Lett.* **78** (1997) 610–613, [hep-ph/9603249].
 - [7] X. Ji, X. Xiong and F. Yuan, *Proton Spin Structure from Measurable Parton Distributions*, *Phys. Rev. Lett.* **109** (2012) 152005, [1202.2843].
 - [8] E. Leader and C. Lorce, *The angular momentum controversy: What's it all about and does it matter?*, *Phys.Rept.* **541** (2014) 163–248, [1309.4235].
 - [9] Y. V. Kovchegov, D. Pitonyak and M. D. Sievert, *Helicity Evolution at Small-x*, *JHEP* **01** (2016) 072, [1511.06737].
 - [10] Y. V. Kovchegov and M. D. Sievert, *Calculating TMDs of a Large Nucleus: Quasi-Classical Approximation and Quantum Evolution*, *Nucl. Phys.* **B903** (2016) 164–203, [1505.01176].
 - [11] I. Balitsky, *Operator expansion for high-energy scattering*, *Nucl. Phys.* **B463** (1996) 99–160, [hep-ph/9509348].
 - [12] I. Balitsky, *Factorization and high-energy effective action*, *Phys. Rev.* **D60** (1999) 014020, [hep-ph/9812311].
 - [13] Y. V. Kovchegov, *Small-x F₂ structure function of a nucleus including multiple pomeron exchanges*, *Phys. Rev.* **D60** (1999) 034008, [hep-ph/9901281].
 - [14] Y. V. Kovchegov, *Unitarization of the BFKL pomeron on a nucleus*, *Phys. Rev.* **D61** (2000) 074018, [hep-ph/9905214].
 - [15] J. Jalilian-Marian, A. Kovner and H. Weigert, *The Wilson renormalization group for low x physics: Gluon evolution at finite parton density*, *Phys. Rev.* **D59** (1998) 014015, [hep-ph/9709432].
 - [16] J. Jalilian-Marian, A. Kovner, A. Leonidov and H. Weigert, *The Wilson renormalization group for low x physics: Towards the high density regime*, *Phys. Rev.* **D59** (1998) 014014, [hep-ph/9706377].
 - [17] E. Iancu, A. Leonidov and L. D. McLerran, *The renormalization group equation for the color glass condensate*, *Phys. Lett.* **B510** (2001) 133–144.

- [18] E. Iancu, A. Leonidov and L. D. McLerran, *Nonlinear gluon evolution in the color glass condensate. I*, *Nucl. Phys.* **A692** (2001) 583–645, [[hep-ph/0011241](#)].
- [19] E. A. Kuraev, L. N. Lipatov and V. S. Fadin, *The Pomeron singularity in non-Abelian gauge theories*, *Sov. Phys. JETP* **45** (1977) 199–204.
- [20] I. Balitsky and L. Lipatov, *The Pomeron singularity in Quantum Chromodynamics*, *Sov.J.Nucl.Phys.* **28** (1978) 822–829.
- [21] R. Kirschner and L. Lipatov, *Double Logarithmic Asymptotics and Regge Singularities of Quark Amplitudes with Flavor Exchange*, *Nucl.Phys.* **B213** (1983) 122–148.
- [22] R. Kirschner, *Regge Asymptotics of Scattering Amplitudes in the Logarithmic Approximation of QCD*, *Z. Phys.* **C31** (1986) 135.
- [23] R. Kirschner, *Regge asymptotics of scattering with flavor exchange in QCD*, *Z.Phys.* **C67** (1995) 459–466, [[hep-th/9404158](#)].
- [24] R. Kirschner, *Reggeon interactions in perturbative QCD*, *Z.Phys.* **C65** (1995) 505–510, [[hep-th/9407085](#)].
- [25] S. Griffiths and D. Ross, *Studying the perturbative Reggeon*, *Eur.Phys.J.* **C12** (2000) 277–286, [[hep-ph/9906550](#)].
- [26] K. Itakura, Y. V. Kovchegov, L. McLerran and D. Teaney, *Baryon stopping and valence quark distribution at small x* , *Nucl. Phys.* **A730** (2004) 160–190, [[hep-ph/0305332](#)].
- [27] J. Bartels and M. Lublinsky, *Quark anti-quark exchange in $\gamma^* \gamma^*$ scattering*, *JHEP* **0309** (2003) 076, [[hep-ph/0308181](#)].
- [28] J. Bartels, B. Ermolaev and M. Ryskin, *Nonsinglet contributions to the structure function g_1 at small x* , *Z.Phys.* **C70** (1996) 273–280, [[hep-ph/9507271](#)].
- [29] J. Bartels, B. Ermolaev and M. Ryskin, *Flavor singlet contribution to the structure function $G(1)$ at small x* , *Z.Phys.* **C72** (1996) 627–635, [[hep-ph/9603204](#)].
- [30] B. I. Ermolaev, M. Greco and S. I. Troian, *QCD running coupling effects for the nonsinglet structure function at small x* , *Nucl. Phys.* **B571** (2000) 137–150, [[hep-ph/9906276](#)].
- [31] B. I. Ermolaev, M. Greco and S. I. Troyan, *Intercepts of the nonsinglet structure functions*, *Nucl. Phys.* **B594** (2001) 71–88, [[hep-ph/0009037](#)].
- [32] B. I. Ermolaev, M. Greco and S. I. Troyan, *Running coupling effects for the singlet structure function g_1 at small x* , *Phys. Lett.* **B579** (2004) 321–330, [[hep-ph/0307128](#)].
- [33] B. I. Ermolaev, M. Greco and S. I. Troyan, *Overview of the spin structure function g_1 at arbitrary x and Q^2* , *Riv. Nuovo Cim.* **33** (2010) 57–122, [[0905.2841](#)].
- [34] A. H. Mueller, *Soft gluons in the infinite momentum wave function and the BFKL pomeron*, *Nucl. Phys.* **B415** (1994) 373–385.
- [35] A. H. Mueller and B. Patel, *Single and double BFKL pomeron exchange and a dipole picture of high-energy hard processes*, *Nucl. Phys.* **B425** (1994) 471–488, [[hep-ph/9403256](#)].
- [36] A. H. Mueller, *Unitarity and the BFKL pomeron*, *Nucl. Phys.* **B437** (1995) 107–126, [[hep-ph/9408245](#)].
- [37] Y. V. Kovchegov, D. Pitonyak and M. D. Sievert, *Helicity Evolution at Small x : Flavor Singlet and Non-Singlet Observables*, *Phys. Rev.* **D95** (2017) 014033, [[1610.06197](#)].
- [38] Y. V. Kovchegov, D. Pitonyak and M. D. Sievert, *Small- x asymptotics of the quark helicity distribution*, *Phys. Rev. Lett.* **118** (2017) 052001, [[1610.06188](#)].
- [39] Y. V. Kovchegov, D. Pitonyak and M. D. Sievert, *Small- x Asymptotics of the Quark Helicity Distribution: Analytic Results*, **1703.05809**.
- [40] F. Dominguez, C. Marquet, B.-W. Xiao and F. Yuan, *Universality of Unintegrated Gluon Distributions at small x* , *Phys.Rev.* **D83** (2011) 105005, [[1101.0715](#)].
- [41] A. Metz and J. Zhou, *Distribution of linearly polarized gluons inside a large nucleus*, *Phys.Rev.* **D84** (2011) 051503, [[1105.1991](#)].
- [42] F. Dominguez, A. Mueller, S. Munier and B.-W. Xiao, *On the small- x evolution of the color quadrupole and the Weizsäcker-Williams gluon distribution*, *Phys.Lett.* **B705** (2011) 106–111, [[1108.1752](#)].
- [43] D. de Florian, R. Sassot, M. Stratmann and W. Vogelsang, *Evidence for polarization of gluons in the proton*, *Phys. Rev. Lett.* **113** (2014) 012001, [[1404.4293](#)].
- [44] P. J. Mulders and R. D. Tangerman, *The Complete tree level result up to order $1/Q$ for polarized deep inelastic lepton production*, *Nucl. Phys.* **B461** (1996) 197–237, [[hep-ph/9510301](#)].
- [45] G. Beuf, *Improving the kinematics for low- x QCD evolution equations in coordinate space*, *Phys. Rev.* **D89** (2014) 074039, [[1401.0313](#)].
- [46] A. H. Mueller, *Small x Behavior and Parton Saturation: A QCD Model*, *Nucl. Phys.* **B335** (1990) 115.
- [47] Y. V. Kovchegov and E. Levin, *Quantum chromodynamics at high energy*, vol. 33. Cambridge University Press, 2012.
- [48] P. J. Mulders and J. Rodrigues, *Transverse momentum dependence in gluon distribution and fragmentation functions*, *Phys. Rev.* **D63** (2001) 094021, [[hep-ph/0009343](#)].
- [49] J. C. Collins and D. E. Soper, *Parton Distribution and Decay Functions*, *Nucl.Phys.* **B194** (1982) 445.
- [50] X.-d. Ji, J.-P. Ma and F. Yuan, *Transverse-momentum-dependent gluon distributions and semi-inclusive processes at hadron colliders*, *JHEP* **07** (2005) 020, [[hep-ph/0503015](#)].
- [51] C. J. Bomhof, P. J. Mulders and F. Pijlman, *The Construction of gauge-links in arbitrary hard processes*, *Eur. Phys. J.* **C47** (2006) 147–162, [[hep-ph/0601171](#)].
- [52] M. D. Sievert, *Transverse Spin and Classical Gluon Fields: Combining Two Perspectives on Hadronic Structure*, **1407.4047**.
- [53] Y. Hatta, Y. Nakagawa, F. Yuan, Y. Zhao and B. Xiao, *Gluon orbital angular momentum at small- x* , *Phys. Rev.* **D95**

- (2017) 114032, [1612.02445].
- [54] G. A. Chirilli, Y. V. Kovchegov and D. E. Wertepny, *Regularization of the Light-Cone Gauge Gluon Propagator Singularities Using Sub-Gauge Conditions*, *JHEP* **12** (2015) 138, [1508.07962].
 - [55] Y. V. Kovchegov, *Non-abelian Weizsäcker-Williams field and a two-dimensional effective color charge density for a very large nucleus*, *Phys. Rev.* **D54** (1996) 5463–5469, [hep-ph/9605446].
 - [56] Y. V. Kovchegov, *Quantum structure of the non-Abelian Weizsäcker-Williams field for a very large nucleus*, *Phys. Rev.* **D55** (1997) 5445–5455, [hep-ph/9701229].
 - [57] I. Balitsky and A. Tarasov, *Rapidity evolution of gluon TMD from low to moderate x* , *JHEP* **10** (2015) 017, [1505.02151].
 - [58] A. Mueller and S. Munier, *p_\perp -broadening and production processes versus dipole/quadrupole amplitudes at next-to-leading order*, *Nucl. Phys.* **A893** (2012) 43–86, [1206.1333].
 - [59] Y. V. Kovchegov and M. D. Sievert, *Small- x Helicity Evolution: an Operator Treatment*, 1808.09010.
 - [60] E. Iancu, J. D. Madrigal, A. H. Mueller, G. Soyez and D. N. Triantafyllopoulos, *Resumming double logarithms in the QCD evolution of color dipoles*, *Phys. Lett.* **B744** (2015) 293–302, [1502.05642].
 - [61] A. H. Mueller, *Unitarity and the BFKL pomeron*, *Nucl. Phys.* **B437** (1995) 107–126, [hep-ph/9408245].
 - [62] STAR collaboration, L. Adamczyk et al., *Precision Measurement of the Longitudinal Double-spin Asymmetry for Inclusive Jet Production in Polarized Proton Collisions at $\sqrt{s} = 200$ GeV*, *Phys. Rev. Lett.* **115** (2015) 092002, [1405.5134].
 - [63] PHENIX collaboration, A. Adare et al., *Inclusive cross section and double-helicity asymmetry for π^0 production at midrapidity in $p+p$ collisions at $\sqrt{s} = 510$ GeV*, *Phys. Rev.* **D93** (2016) 011501, [1510.02317].
 - [64] E. C. Aschenauer, R. Sassot and M. Stratmann, *Unveiling the Proton Spin Decomposition at a Future Electron-Ion Collider*, *Phys. Rev.* **D92** (2015) 094030, [1509.06489].
 - [65] D. de Florian, R. Sassot, M. Stratmann and W. Vogelsang, *Extraction of Spin-Dependent Parton Densities and Their Uncertainties*, *Phys. Rev.* **D80** (2009) 034030, [0904.3821].
 - [66] P. Jimenez-Delgado, A. Accardi and W. Melnitchouk, *Impact of hadronic and nuclear corrections on global analysis of spin-dependent parton distributions*, *Phys. Rev.* **D89** (2014) 034025, [1310.3734].
 - [67] JEFFERSON LAB ANGULAR MOMENTUM collaboration, N. Sato, W. Melnitchouk, S. E. Kuhn, J. J. Ethier and A. Accardi, *Iterative Monte Carlo analysis of spin-dependent parton distributions*, *Phys. Rev.* **D93** (2016) 074005, [1601.07782].
 - [68] J. J. Ethier, N. Sato and W. Melnitchouk, *First simultaneous extraction of spin-dependent parton distributions and fragmentation functions from a global QCD analysis*, 1705.05889.
 - [69] E. Leader, A. V. Sidorov and D. B. Stamenov, *Longitudinal polarized parton densities updated*, *Phys. Rev.* **D73** (2006) 034023, [hep-ph/0512114].
 - [70] E. Leader, A. V. Sidorov and D. B. Stamenov, *Determination of Polarized PDFs from a QCD Analysis of Inclusive and Semi-inclusive Deep Inelastic Scattering Data*, *Phys. Rev.* **D82** (2010) 114018, [1010.0574].
 - [71] E. Leader, A. V. Sidorov and D. B. Stamenov, *New analysis concerning the strange quark polarization puzzle*, *Phys. Rev.* **D91** (2015) 054017, [1410.1657].
 - [72] NNPDF collaboration, R. D. Ball, S. Forte, A. Guffanti, E. R. Nocera, G. Ridolfi and J. Rojo, *Unbiased determination of polarized parton distributions and their uncertainties*, *Nucl. Phys.* **B874** (2013) 36–84, [1303.7236].
 - [73] NNPDF collaboration, E. R. Nocera, R. D. Ball, S. Forte, G. Ridolfi and J. Rojo, *A first unbiased global determination of polarized PDFs and their uncertainties*, *Nucl. Phys.* **B887** (2014) 276–308, [1406.5539].
 - [74] Y. L. Dokshitzer, *Calculation of the Structure Functions for Deep Inelastic Scattering and e^+e^- Annihilation by Perturbation Theory in Quantum Chromodynamics*, *Sov. Phys. JETP* **46** (1977) 641–653.
 - [75] V. N. Gribov and L. N. Lipatov, *Deep inelastic $e p$ scattering in perturbation theory*, *Sov. J. Nucl. Phys.* **15** (1972) 438–450.
 - [76] G. Altarelli and G. Parisi, *Asymptotic Freedom in Parton Language*, *Nucl. Phys.* **B126** (1977) 298.
 - [77] I. I. Balitsky, *Quark Contribution to the Small- x Evolution of Color Dipole*, *Phys. Rev. D* **75** (2007) 014001, [hep-ph/0609105].
 - [78] E. Gardi, J. Kuokkanen, K. Rummukainen and H. Weigert, *Running coupling and power corrections in nonlinear evolution at the high-energy limit*, *Nucl. Phys.* **A784** (2007) 282–340, [hep-ph/0609087].
 - [79] Y. Kovchegov and H. Weigert, *Triumvirate of Running Couplings in Small- x Evolution*, *Nucl. Phys.* **A 784** (2007) 188–226, [hep-ph/0609090].
 - [80] Y. V. Kovchegov and H. Weigert, *Quark loop contribution to BFKL evolution: Running coupling and leading- $N(f)$ NLO intercept*, *Nucl. Phys.* **A789** (2007) 260–284, [hep-ph/0612071].
 - [81] J. L. Albacete, N. Armesto, J. G. Milhano, C. A. Salgado and U. A. Wiedemann, *Numerical analysis of the Balitsky-Kovchegov equation with running coupling: Dependence of the saturation scale on nuclear size and rapidity*, *Phys. Rev.* **D71** (2005) 014003, [hep-ph/0408216].
 - [82] J. L. Albacete and Y. V. Kovchegov, *Solving high energy evolution equation including running coupling corrections*, *Phys. Rev.* **D75** (2007) 125021, [arXiv:0704.0612 [hep-ph]].
 - [83] J. L. Albacete, N. Armesto, J. G. Milhano and C. A. Salgado, *Non-linear QCD meets data: A global analysis of lepton-proton scattering with running coupling BK evolution*, *Phys. Rev.* **D80** (2009) 034031, [0902.1112].
 - [84] J. L. Albacete, N. Armesto, J. G. Milhano, P. Quiroga-Arias and C. A. Salgado, *AAMQS: A non-linear QCD analysis of new HERA data at small- x including heavy quarks*, *Eur. Phys. J.* **C71** (2011) 1705, [1012.4408].
 - [85] J. Kuokkanen, K. Rummukainen and H. Weigert, *HERA-Data in the Light of Small x Evolution with State of the Art NLO Input*, *Nucl. Phys.* **A875** (2012) 29–93, [1108.1867].